THE ASTROPHYSICAL JOURNAL, ???:??–??, 2006 ???, ASTRO-PH/0602442
Preprint typeset using LaTeX style emulateapj v. 12/14/05

CHANDRA OBSERVATIONS OF THE HIGHEST REDSHIFT QUASARS FROM THE SLOAN DIGITAL SKY SURVEY

OHAD SHEMMER,[1] W. N. BRANDT,[1] DONALD P. SCHNEIDER,[1] XIAOHUI FAN,[2] MICHAEL A. STRAUSS,[3]
ALEKSANDAR M. DIAMOND-STANIC,[2] GORDON T. RICHARDS,[3] SCOTT F. ANDERSON,[4] JAMES E. GUNN,[3]
AND JON BRINKMANN[5]

Received 2006 January 6; accepted 2006 February 17

ABSTRACT

We present new *Chandra* observations of 21 $z > 4$ quasars, including 11 sources at $z > 5$. These observations double the number of X-ray detected quasars at $z > 5$, allowing investigation of the X-ray spectral properties of a substantial sample of quasars at the dawn of the modern Universe. By jointly fitting the spectra of 15 $z > 5$ radio-quiet quasars (RQQs), including sources from the *Chandra* archive, with a total of 185 photons, we find a mean X-ray power-law photon index of $\Gamma = 1.95^{+0.30}_{-0.26}$, and a mean neutral intrinsic absorption column density of $N_{\rm H} \lesssim 6\times10^{22}\,{\rm cm}^{-2}$. These results show that quasar X-ray spectral properties have not evolved up to the highest observable redshifts. We also find that the mean optical–X-ray spectral slope ($\alpha_{\rm ox}$) of optically-selected $z > 5$ RQQs, excluding broad absorption line quasars, is $\alpha_{\rm ox} = -1.69 \pm 0.03$, which is consistent with the value predicted from the observed relationship between $\alpha_{\rm ox}$ and ultraviolet luminosity. Four of the sources in our sample are members of the rare class of weak emission-line quasars, and we detect two of them in X-rays. We discuss the implications our X-ray observations have for the nature of these mysterious sources and, in particular, whether their weak-line spectra are a consequence of continuum boosting or a deficit of high-ionization line emitting gas.

Subject headings: galaxies: active – galaxies: nuclei – X-rays: galaxies – quasars: general – quasars: emission lines

1. INTRODUCTION

During the past five years over 100 quasars at $z > 4$ have been detected in X-rays[6], probing the inner regions of active galactic nuclei (AGNs) when the Universe was $\lesssim 1.5$ Gyr old (e.g., Kaspi et al. 2000; Brandt et al. 2002; Bechtold et al. 2003; Vignali et al. 2003a, 2003b, 2005; Shemmer et al. 2005). Those studies have provided measurements of the X-ray power-law photon index, intrinsic absorption column density, and the optical–X-ray spectral energy distribution (SED) of a few $z > 4$ quasars which are particularly bright in X-rays, as well as the mean properties of large samples of these sources via joint fitting of their X-ray spectra (e.g., Page et al. 2005; Shemmer et al. 2005; Vignali et al. 2003a, 2003b, 2005). The results demonstrated that the X-ray spectra of $z > 4$ quasars do not differ significantly from those of AGNs at lower redshift, and that the X-ray photon index of AGNs does not depend on luminosity (but see also Bechtold et al. 2003; Dai et al. 2004; Grupe et al. 2006). This is generally consistent with recent observations showing that the longer wavelength SEDs of quasars have not significantly evolved over cosmic time (e.g., see Stern et al. 2000, Carilli et al. 2001, and Petric et al. 2003 for radio observations and Schneider, Schmidt, & Gunn 1991, Vanden Berk et al. 2001, and Pentericci et al. 2003 for rest-frame optical–ultraviolet (UV) observations). While the X-ray spectral properties of $4 < z < 5$ quasars are now fairly well established, the situation for quasars at the highest observable redshifts, $z > 5$, is not yet as clear. Only loose constraints on the typical X-ray spectral properties of $z > 5$ quasars are available, mainly due to the small number of such sources discovered so far ($\lesssim 50$). Obtaining X-ray spectral information for the highest-redshift quasars is important for understanding the physical processes and environments of AGNs at the end of the reionization epoch (e.g., Loeb & Barkana 2001).

X-ray observations of $z > 5$ quasars are challenging for present-day X-ray missions such as the *Chandra* X-ray Observatory and *XMM-Newton*. Typically, exposure times of ≈ 10 ks or more are required to detect ~ 5 photons from these sources, and $\gtrsim 100$ ks is required to obtain a reliable measurement of the photon index (Farrah et al. 2004; Schwartz & Virani 2004). Prior to this work, only 11 quasars (10 of which are radio quiet, and one that is radio loud) at $z > 5$ had been X-ray detected (Brandt et al. 2001, 2002; Vignali et al. 2001, 2002, 2003b; Barger et al. 2002; Mathur et al. 2002; Bechtold et al. 2003; Steffen et al. 2004). In this work we add 11 more X-ray detections of $z > 5$ quasars[7] and create a statistically meaningful sample to investigate the mean X-ray properties of these sources. In addition, we present new X-ray observations of four $z \sim 4.5$ sources which belong to the rare class of weak (or absent) emission-line quasars (hereafter WLQs); only about a dozen sources of this type have been discovered at $z > 2$ (e.g., Fan et al. 1999; Anderson et al. 2001; Collinge et al. 2005; Schneider et al. 2005).

This paper is organized as follows: in § 2 we describe the *Chandra* observations and their reduction; the results are presented in § 3. In § 4 we provide notes on individual interesting sources in our sample. In § 5 we discuss the mean X-ray spectral properties of $z > 5$ quasars. In § 6 we discuss the

[1] Department of Astronomy & Astrophysics, The Pennsylvania State University, University Park, PA 16802; ohad@astro.psu.edu
[2] Steward Observatory, University of Arizona, 933 North Cherry Avenue, Tucson, AZ 85721
[3] Princeton University Observatory, Peyton Hall, Princeton, NJ 08544
[4] Department of Astronomy, University of Washington, Box 351580, Seattle, WA 98195
[5] Apache Point Observatory, P.O. Box 59, Sunspot, NM 88349-0059

[6] See http://www.astro.psu.edu/users/niel/papers/highz-xray-detected.dat for a regularly updated compilation of X-ray detections at $z > 4$.

[7] The X-ray detections of two of these sources, SDSS J1053+5804 and SDSS J2228−0757, were reported briefly by Schneider et al. (2005); here we provide a full description of their detections (see § 3).

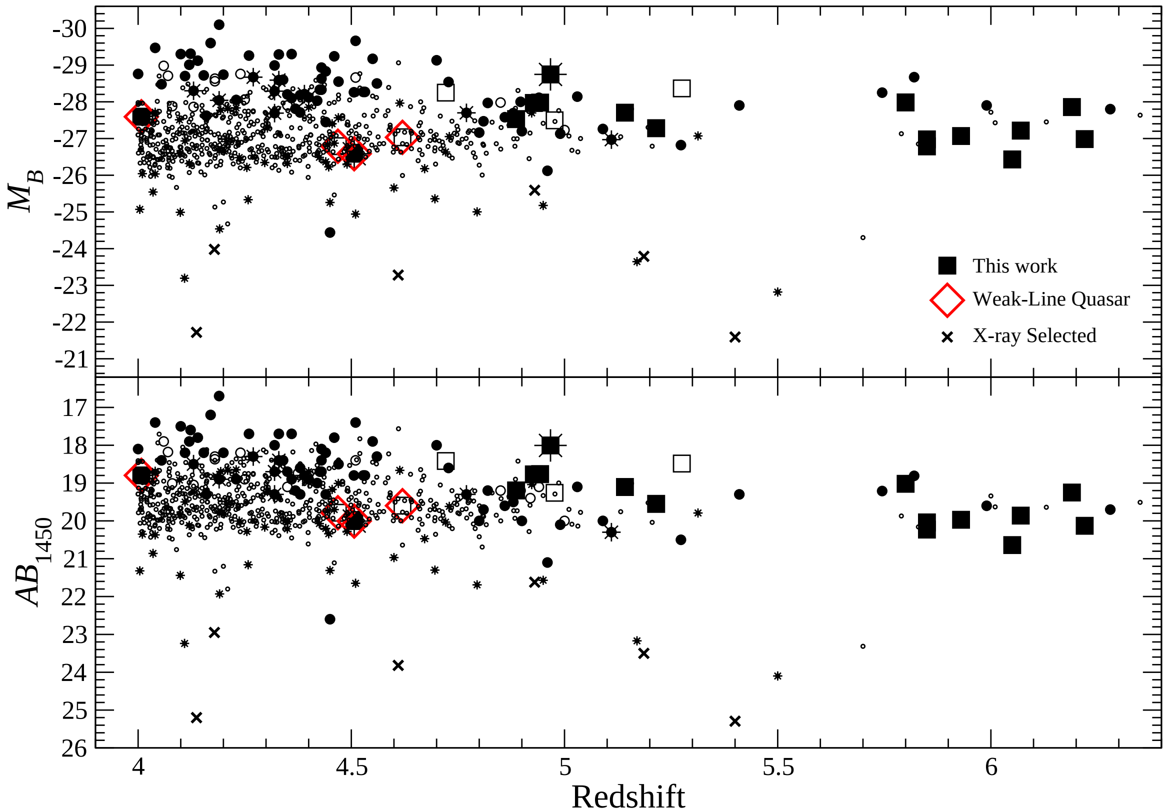

FIG. 1.— $M_{\rm B}$ (*top*) and AB_{1450} (*bottom*) vs. redshift for all published $z>4$ quasars (data were compiled from this work, Bassett et al. 2004, Steffen et al. 2004, Mahabal et al. 2005, Vignali et al. 2005, and Fan et al. 2006). Large symbols indicate X-ray targeted quasars. Open symbols indicate targeted quasars that are X-ray-undetected, but have meaningful upper limits (i.e., $\alpha_{\rm ox}<-1.50$). Stars indicate RLQs and radio-moderate quasars. Squares indicate sources from this work, and enclosing diamonds indicate the WLQs in our sample. Note that two other $z>4$ WLQs, SDSS J0040−0915 (Schneider et al. 2003) and SDSS J133550.81+353315.8 (Fan et al. 2006), are not marked with an enclosing diamond, for clarity.

results of our X-ray observations of WLQs, and how they may shed light on the nature of these sources. A summary of our main results is given in § 7. Complete quasar names are given in the tables and in the headers of § 4, and their abbreviated versions are used throughout the text. Luminosity distances in the paper are determined using the standard cosmological model with parameters $\Omega_\Lambda=0.7$, $\Omega_M=0.3$, and $H_0=70\,{\rm km\,s^{-1}\,Mpc^{-1}}$ (e.g., Spergel et al. 2003).

2. SAMPLE SELECTION, OBSERVATIONS, AND DATA REDUCTION

We have targeted some of the optically brightest quasars at $z\gtrsim5$ (see Fig. 1) to investigate quasar X-ray spectral properties and optical–X-ray SEDs at the highest observable redshifts. Targets with $z\lesssim5.4$ were mostly selected from the Sloan Digital Sky Survey (SDSS; York et al. 2000) Data Release 3 (DR3) quasar catalog (Schneider et al. 2005). Quasars at higher redshifts cannot be detected with the SDSS quasar-selection algorithm (Richards et al. 2002), since Lyα shifts from the *i* band to the *z* band, and detections require the aid of near-infrared (IR) imaging and spectroscopy (e.g., Fan et al. 2004). We obtained short (∼3–30 ks) X-ray observations of 19 of the most distant quasars known with *Chandra* during Cycles 4 and 6 (see Fig. 1). The observation log appears in Table 1, where we also list references to the quasars' discovery papers. The targets include 18 newly discovered quasars from the SDSS survey (12 of which appear in the DR3 catalog; Schneider et al. 2005) and one previously X-ray-targeted quasar, SDSS J1532−0039 at $z=4.62$, which is the prototype of the WLQ class (Fan et al. 1999; Vignali et al. 2001). Three other WLQs from DR3 are included in our sample; our aim is to utilize the X-ray data to shed light on the nature of these sources. Our sample includes one radio-loud quasar (RLQ), SDSS J0011+1446, and two broad absorption line quasars (BALQSOs), SDSS J1048+4637 and SDSS J1653+4054. The Cycle 4 and 6 sources were observed with the Advanced CCD Imaging Spectrometer (ACIS; Garmire et al. 2003) with the S3 CCD at the aimpoint. In addition, we add to our sample serendipitous *Chandra* detections of two $z>4$ quasars, SDSS J1026+4719 at $z=4.94$ from Cycle 1, and SDSS J1053+5804 at $z=5.21$ from Cycle 2 (see Table 1); both of these sources were observed with ACIS-I and lie near the edge of the field of view.

Faint mode was used for the event telemetry format in all the observations, and *ASCA* grade 0, 2, 3, 4, and 6 events were used in the analysis, which was carried out using standard CIAO[8] v3.2 routines. No background flares are present in these observations. Source detection was carried out with WAVDETECT (Freeman et al. 2002) using wavelet transforms (with wavelet scale sizes of 1, 1.4, 2, 2.8, and 4 pixels) and a false-positive probability threshold of 10^{-4}. Given the small number of pixels being searched due to the accurate a priori source positions and the subarcsecond on-axis angular resolution of *Chandra*, the probability of spurious detections is extremely low; most of the sources were in fact detected at a false-positive probability threshold of 10^{-6}.

The X-ray counts detected in the ultrasoft band

[8] *Chandra* Interactive Analysis of Observations. See http://asc.harvard.edu/ciao/

TABLE 1
Chandra OBSERVATIONS LOG

Object (SDSS J)	z	$\Delta_{\rm Opt-X}$[a] (arcsec)	X-ray Obs. Date	*Chandra* Cycle no.	Exp. Time[b] (ks)	Ref.	Notes
000239.39+255034.8	5.80	0.3	2005 Jan 24	6	5.87	1	
000552.34−000655.8	5.85	0.4	2005 Jul 28	6	16.93	1	
001115.23+144601.8	4.97	0.3	2003 May 20	4	3.49	2	
084035.09+562419.9	5.85	0.2	2005 Feb 3–4	6	15.84	3	
102622.89+471907.0	4.94	1.6	2000 June 7–8	1	2.29[e]	2	Off-axis on ACIS-I
104845.05+463718.3	6.19	0.3	2005 Jan 10	6	14.97	4	Broad absorption line quasar
105322.98+580412.1	5.21	0.8	2001 July 5	2	4.70[e]	2	Off-axis on ACIS-I
130216.13+003032.1	4.47	···	2003 May 17	4	10.81	2	Weak emission lines
140850.91+020522.7	4.01	0.5	2005 Mar 02	6	6.00	2	Weak emission lines
141111.29+121737.4	5.93	0.2	2005 Mar 17	6	14.27	1	
143352.20+022713.9	4.72	···	2003 Apr 20	4	3.50	2	
144231.72+011055.2	4.51	0.3	2002 Dec 16	4	11.01	2	Weak emission lines
153259.96−003944.1[c]	4.62	···	2005 Apr 2	6	9.83	5	Weak emission lines
153650.26+500810.3	4.93	0.2	2005 Sep 23	6	4.62	2	
160253.98+422824.9[d]	6.07	0.3	2005 Oct 29	6	13.20	1	
162331.81+311200.5	6.22	0.5	2004 Dec 29	6	17.21	1	Strong Lyα
162626.50+275132.4	5.28	···	2005 May 12–13	6	4.82	2	
163033.90+401209.6	6.05	0.1	2005 Nov 4	6	27.39	4	
165354.61+405402.1	4.98	···	2002 Dec 8–9	4	3.12	2	Broad absorption line quasar
222509.19−001406.8	4.89	0.4	2003 Sep 10–11	4	3.45	2	
222845.14−075755.3	5.14	0.7	2003 May 5	4	7.04	2	

REFERENCES. — (1) Fan et al. (2004); (2) Schneider et al. (2005); (3) Fan et al. (2006); (4) Fan et al. (2003); (5) Fan et al. (1999).

NOTE. — The optical positions of the quasars have been obtained from the reference given in the seventh column, and the X-ray positions have been obtained with WAVDETECT.

[a] Distance between the optical and X-ray positions; missing values indicate no X-ray detection.
[b] The *Chandra* exposure time has been corrected for detector dead time.
[c] An additional 5.09 ks *Chandra* exposure of the source is included in the current analysis, raising the total exposure time to 14.92 ks (see Vignali et al. 2001 and § 2 for details).
[d] The optical coordinates of this source from Fan et al. (2004) have been corrected using the SDSS DR4 astrometry.
[e] Actual exposure time, not corrected by the exposure map.

(0.3–0.5 keV), the soft band (0.5–2 keV), the hard band (2–8 keV), and the full band (0.5–8 keV) are reported in Table 2. The counts were derived from manual aperture photometry, and they are consistent with the photometry obtained using WAVDETECT. Sixteen quasars were detected with 2–127 full-band counts; the largest number of counts was obtained from SDSS J0011+1446 which is a RLQ. The X-ray positions of the 14 targeted and detected sources differ by $0.2''$–$0.7''$ from their optical positions; the X-ray positions of the two serendipitous, off-axis detections differ by $0.8''$–$1.6''$ from their optical positions (Table 1). These results are consistent with the expected *Chandra* ACIS positional errors. We used the WAVDETECT tool a second time on the fields of the five undetected sources, with a false-positive probability threshold of 10^{-3}, but none of the five sources was detected even at this lower significance level. Table 2 also includes the band ratio, calculated as the counts in the hard band divided by the counts in the soft band, and the effective power-law photon index (Γ, where $N(E) \propto E^{-\Gamma}$; Γ was calculated from the band ratio using the *Chandra* PIMMS v3.6a tool[9]) for each source. For the Cycle 4 and 6 sources the photon index was corrected for the quantum-efficiency decay of ACIS at low energies, caused by molecular contamination of the ACIS filters, using a time-dependent correction calculated with PIMMS.

Figure 2 presents the full-band *Chandra* images of the $50''\times50''$ fields of all 21 quasars. The images of the 12 detected quasars with >3 counts were adaptively smoothed using the algorithm of Ebeling et al. (2006). The images of the four detected sources with ≤ 3 counts, and the images of the fields of the five undetected quasars, were not smoothed; for these objects the raw images are shown. We note that the image of SDSS J1532−0039 was merged with an archival 5.09 ks *Chandra* exposure, centered on the optical position of the source, that did not provide an X-ray detection (Vignali et al. 2001); the merged image, which represents a total exposure time of 14.92 ks, is shown in Fig. 2. Inspection of the *Chandra* images of our bright quasars does not reveal any excess X-ray emission in their vicinity that might be interpreted as gravitationally lensed images (e.g., Wyithe & Loeb 2002; Richards et al. 2006) or jets (e.g., Schwartz 2002; Schwartz & Virani 2004).

With the exception of SDSS J0005−0006, we did not find any significant excess of companions with respect to the cumulative number counts from X-ray surveys (e.g., Bauer et al. 2004) in the $\approx 300\times300\,{\rm kpc}^2$ projected regions centered on the quasar positions; this is in agreement with previous X-ray searches around high-z quasars (e.g., Vignali et al. 2005 and references therein). A bright X-ray source, with $\sim$60 full-band counts, is apparent in the *Chandra* image of SDSS J0005−0006 with an angular distance of $\sim 20''$ from the target (Fig. 2). This source is classified as a galaxy in the SDSS DR4 catalog (Adelman-McCarthy et al. 2006), but due to its faintness ($i = 22.1$) an SDSS spectrum is not available. The X-ray-to-optical flux ratio of the source is just $\sim$3 times lower than the relatively high X-ray-to-optical flux ratio of SDSS J0005−0006 (see Table 3, placed at the end of the paper), and based upon photometry using co-added SDSS images in this area (Jiang et al. 2006) its photometric redshift is $z = 0.575 \pm 0.175$ with an integrated probability of 63% (Weinstein et al. 2004). Given this redshift we calculate an X-ray luminosity in the rest-frame 2–10 keV band of $\approx 10^{43}\,{\rm erg\,s^{-1}}$

[9] See http://cxc.harvard.edu/toolkit/pimms.jsp

TABLE 2
X-RAY COUNTS, BAND RATIOS, AND EFFECTIVE PHOTON INDICES

Object	X-ray Counts[a]					
(SDSS J)	0.3–0.5 keV	0.5–2 keV	2–8 keV	0.5–8 keV	Band Ratio[b]	Γ[b]
000239.39+255034.8	<4.8	$5.0^{+3.4}_{-2.2}$	<3.0	$5.0^{+3.4}_{-2.2}$	<0.60	>1.2
000552.34−000655.8	<3.0	$16.4^{+5.1}_{-4.0}$	<3.0	$17.6^{+5.3}_{-4.1}$	<0.18	>2.2
001115.23+144601.8	$6.9^{+3.8}_{-2.6}$	$98.1^{+10.9}_{-9.9}$	$28.8^{+6.4}_{-5.3}$	$126.9^{+12.3}_{-11.2}$	$0.29^{+0.07}_{-0.06}$	$1.7^{+0.2}_{-0.2}$
084035.09+562419.9	<3.0	$3.0^{+2.9}_{-1.6}$	<4.8	$3.0^{+2.9}_{-1.6}$	<1.60	>0.3
102622.89+471907.0	<3.0	$3.7^{+3.1}_{-1.8}$	<6.4	$5.3^{+3.5}_{-2.2}$	<1.73	>0.2
104845.05+463718.3	<3.0	$3.0^{+2.9}_{-1.6}$	<3.0	$3.0^{+2.9}_{-1.6}$	<1.00	>0.7
105322.98+580412.1	<3.0	$3.7^{+3.1}_{-1.8}$	<4.8	$4.3^{+3.3}_{-2.0}$	<1.30	>0.5
130216.13+003032.1	<3.0	<4.8	<4.8	<6.4	···	···
140850.91+020522.7	$4.0^{+3.2}_{-1.9}$	$26.2^{+6.2}_{-5.1}$	$4.0^{+3.2}_{-1.9}$	$30.0^{+6.5}_{-5.4}$	$0.15^{+0.13}_{-0.08}$	$2.4^{+0.7}_{-0.6}$
141111.29+121737.4	<4.8	$10.9^{+4.4}_{-3.3}$	<6.4	$12.9^{+4.7}_{-3.5}$	<0.59	>1.2
143352.20+022713.9	<3.0	<4.8	<3.0	<4.8	···	···
144231.72+011055.2	$2.0^{+2.7}_{-1.3}$	$36.7^{+7.1}_{-6.0}$	$6.9^{+3.8}_{-2.6}$	$43.6^{+7.7}_{-6.6}$	$0.19^{+0.11}_{-0.08}$	$2.0^{+0.4}_{-0.4}$
153259.96−003944.1	<3.0	<3.0	<3.0	<3.0	···	···
153650.26+500810.3	<3.0	$7.0^{+3.8}_{-2.6}$	$8.0^{+4.0}_{-2.8}$	$14.7^{+4.9}_{-3.8}$	$1.15^{+0.70}_{-0.78}$	$0.6^{+1.0}_{-0.5}$
160253.98+422824.9	<4.8	$22.6^{+5.8}_{-4.7}$	$2.9^{+2.9}_{-1.6}$	$26.3^{+6.2}_{-5.1}$	$0.13^{+0.13}_{-0.08}$	$2.5^{+0.8}_{-0.6}$
162331.81+311200.5	<3.0	$2.9^{+2.9}_{-1.6}$	<8.0	$5.7^{+3.5}_{-2.3}$	<2.76	>-0.2
162626.50+275132.4	<3.0	<4.8	<3.0	<4.8	···	···
163033.90+401209.6	$2.0^{+2.7}_{-1.3}$	$13.6^{+4.8}_{-3.6}$	$4.0^{+3.2}_{-1.9}$	$17.4^{+5.3}_{-4.1}$	$0.29^{+0.25}_{-0.18}$	$1.8^{+0.8}_{-0.6}$
165354.61+405402.1	<3.0	<3.0	<6.4	<6.4	···	···
222509.19−001406.8	<3.0	$2.0^{+2.7}_{-1.3}$	<3.0	$2.0^{+2.7}_{-1.3}$	<1.50	>0.2
222845.14−075755.3	<3.0	$2.0^{+2.7}_{-1.3}$	<4.8	$3.0^{+2.9}_{-1.6}$	<2.40	>-0.2

[a]Errors on the X-ray counts were computed according to Tables 1 and 2 of Gehrels (1986) and correspond to the 1σ level; these were calculated using Poisson statistics. The upper limits are at the 95% confidence level and were computed according to Kraft, Burrows, & Nousek (1991). Upper limits of 3.0, 4.8, 6.4, and 8.0 indicate that 0, 1, 2, and 3 X-ray counts, respectively, have been found within an extraction region of radius $1''$ centered on the optical position of the quasar (considering the background within this source-extraction region to be negligible).

[b]We calculated errors at the 1σ level for the band ratio (the ratio between the 2–8 keV and 0.5–2 keV bands) and effective photon index following the "numerical method" described in § 1.7.3 of Lyons (1991); this avoids the failure of the standard approximate-variance formula when the number of counts is small (see § 2.4.5 of Eadie et al. 1971). The photon indices have been obtained applying the correction required to account for the ACIS quantum-efficiency decay at low energy.

for this AGN candidate (the luminosity was obtained in the same way as for the quasars in our sample; see below).

Finally, we searched for rapid variability within the *Chandra* observations of our detected quasars by applying a Kolmogorov-Smirnov test to the photon arrival times, but no significant flux variations were detected. This is not surprising given the combination of the relatively short observations ($\lesssim 1$ hr in the rest-frame) and the small number of detected photons from most of the sources.

3. X-RAY, OPTICAL, AND RADIO PROPERTIES OF THE SAMPLE

The main X-ray, optical, and radio properties of our sample are listed in Table 3:

Column (1). — The SDSS J2000.0 quasar coordinates, accurate to $\sim 0.1''$.

Column (2). — The Galactic column density in units of 10^{20} cm^{-2}, taken from Dickey & Lockman (1990) and obtained with the HEASARC $N_{\rm H}$ tool.[10]

Column (3). — The monochromatic *AB* magnitude at a rest-frame wavelength of 1450 Å ($AB_{1450} = -2.5 \log f_{1450\,\text{Å}} - 48.6$; Oke & Gunn 1983). All the magnitudes have been corrected for Galactic extinction (Schlegel, Finkbeiner, & Davis 1998). In cases where the magnitudes were obtained from the SDSS spectra, a fiber light-loss correction has been applied; this was calculated as the difference between the synthetic *i* magnitude (i.e., the integrated flux across the *i* bandpass in the SDSS spectrum) and the photometric SDSS *i* magnitude, assuming no flux variation between the photometric and spectroscopic epochs.

Column (4). — The absolute *B*-band magnitude, computed assuming a UV–optical power-law slope of $\alpha = -0.5$ ($f_\nu \propto \nu^\alpha$; Vanden Berk et al. 2001).

Columns (5) and (6). — The flux density and luminosity at a rest-frame wavelength of 2500 Å, computed from the magnitudes in Column 3, assuming a UV–optical power-law slope of $\alpha = -0.5$.

Columns (7) and (8). — The count rate in the observed-frame 0.5–2 keV band and the corresponding flux, corrected for Galactic absorption and the quantum-efficiency decay of *Chandra* ACIS at low energy (for the Cycle 4 and 6 sources). The fluxes have been calculated using PIMMS, assuming a power-law model with $\Gamma = 2.0$, which is a typical photon index for luminous AGN with $0 \lesssim z \lesssim 6$ (e.g., Reeves & Turner 2000; Page et al. 2005; Piconcelli et al. 2005; Shemmer et al. 2005; Vignali et al. 2005; see also § 5).

Columns (9) and (10). — The flux density and luminosity at a rest-frame energy of 2 keV, computed assuming $\Gamma = 2.0$ and corrected for the quantum-efficiency decay of *Chandra* ACIS at low energy (for the Cycle 4 and 6 sources).

Column (11). — The luminosity in the rest-frame 2–10 keV band.

Column (12). — The optical–X-ray power-law slope, $\alpha_{\rm ox}$, defined as:

[10] http://heasarc.gsfc.nasa.gov/cgi-bin/Tools/w3nh/w3nh.pl

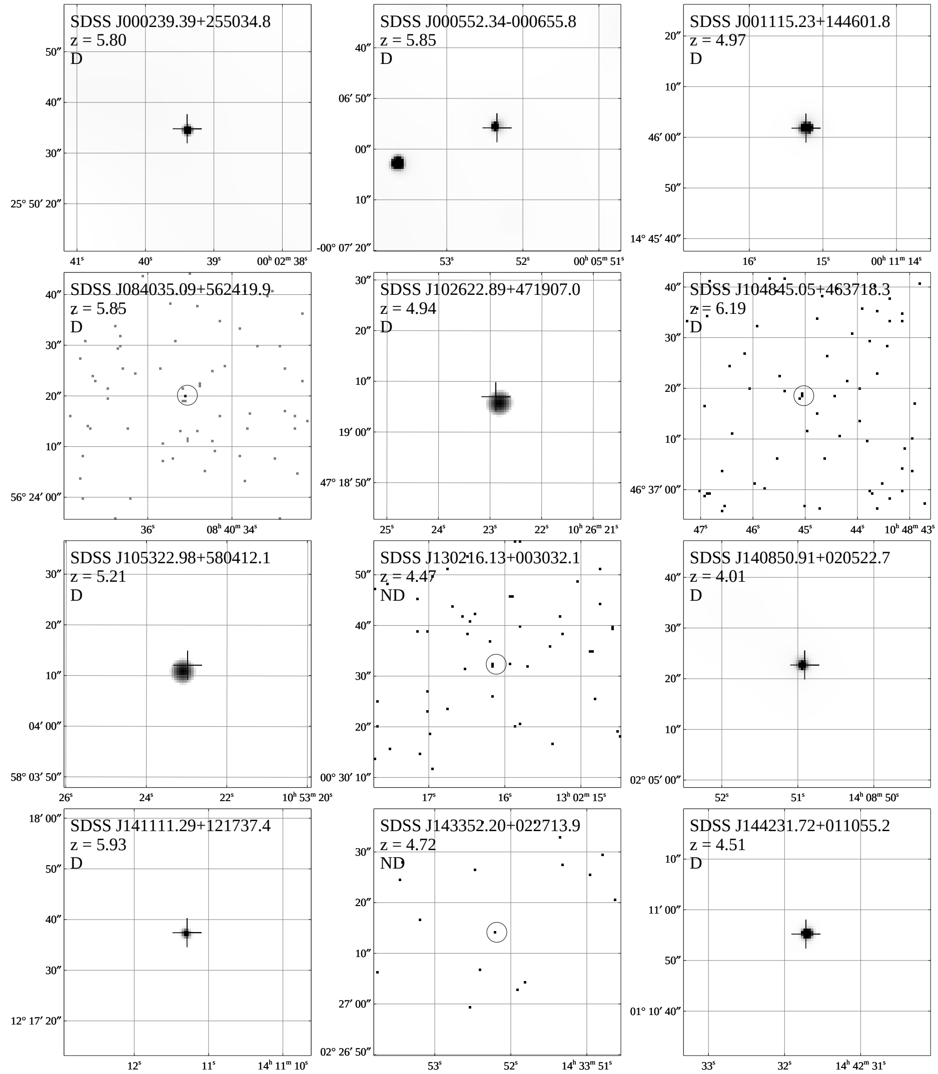

FIG. 2.— Full-band (0.5–8 keV) *Chandra* images of our quasars. Each panel spans $50'' \times 50''$ on the sky; North is up, and East is to the left. The images of the sources with > 3 counts have been adaptively smoothed at the 2σ level; the optical positions of the quasars are marked by crosses. For sources with ≤ 3 counts, the raw (unsmoothed) images and $2''$–radius circles around the optical positions of the quasars are shown. A 'D' ('ND') label in each panel indicates an X-ray detection (non-detection) of the source. Note that the image of SDSS J1532−0039 is a combination of our new Cycle 6 observation and an archival 5.09 ks *Chandra* exposure; the total exposure time for this image is 14.92 ks. The larger offsets between the optical and X-ray positions of the serendipitous sources, SDSS J1026+4719 and SDSS J1053+5804, are due to their large off-axis angles (see § 2).

$$\alpha_{\rm ox} = \frac{\log(f_{2\,\rm keV}/f_{2500\,\text{Å}})}{\log(\nu_{2\,\rm keV}/\nu_{2500\,\text{Å}})} \tag{1}$$

where $f_{2\,\rm keV}$ and $f_{2500\,\text{Å}}$ are the flux densities at rest-frame 2 keV and 2500 Å, respectively. The errors on $\alpha_{\rm ox}$ were computed following the "numerical method" described in § 1.7.3 of Lyons (1991), taking into account the uncertainties in the X-ray count rates and photon indices ($\Gamma = 2.0 \pm 0.1$), and the effects of possible changes in the UV–optical slope (from $\alpha = -0.5$ to $\alpha = -0.79$).

Column (13). — The difference between the measured $\alpha_{\rm ox}$ (from column 12) and the predicted $\alpha_{\rm ox}$, given the UV luminosity from column 6, based on the $\alpha_{\rm ox}$–$L_\nu(2500\,\text{Å})$ relation (given as Eq. 2 of Steffen et al. 2006; see also Strateva et al. 2005). The statistical significance of this difference is also given in units of σ, where $\sigma = 0.146$ for $31 < \log L_\nu(2500\,\text{Å}) < 32$, and $\sigma = 0.131$ for $32 < \log L_\nu(2500\,\text{Å}) < 33$ (see Table 5 of Steffen et al. 2006).

Column (14). — The radio-loudness parameter (e.g., Kellermann et al. 1989), defined as $R = f_{5\,\rm GHz}/f_{4400\,\text{Å}}$ (the ratio of flux densities at rest-frame frequencies). The flux density at a rest-frame frequency of 5 GHz was computed from either the FIRST (Becker, White, & Helfand 1995) or NVSS (Condon et al. 1998) flux densities at an observed-frame frequency of 1.4 GHz, assuming a radio power-law slope of $\alpha = -0.8$. Upper limits on R are at the 3σ level, since the positions of all our sources are known a priori. The flux densities at rest frame 4400 Å were computed from the AB_{1450} magnitudes assuming a UV–optical power-law slope of $\alpha = -0.5$. Typical radio-loudness values are > 100 for RLQs and < 10 for radio-quiet quasars (RQQs). Most of our sources are RQQs.

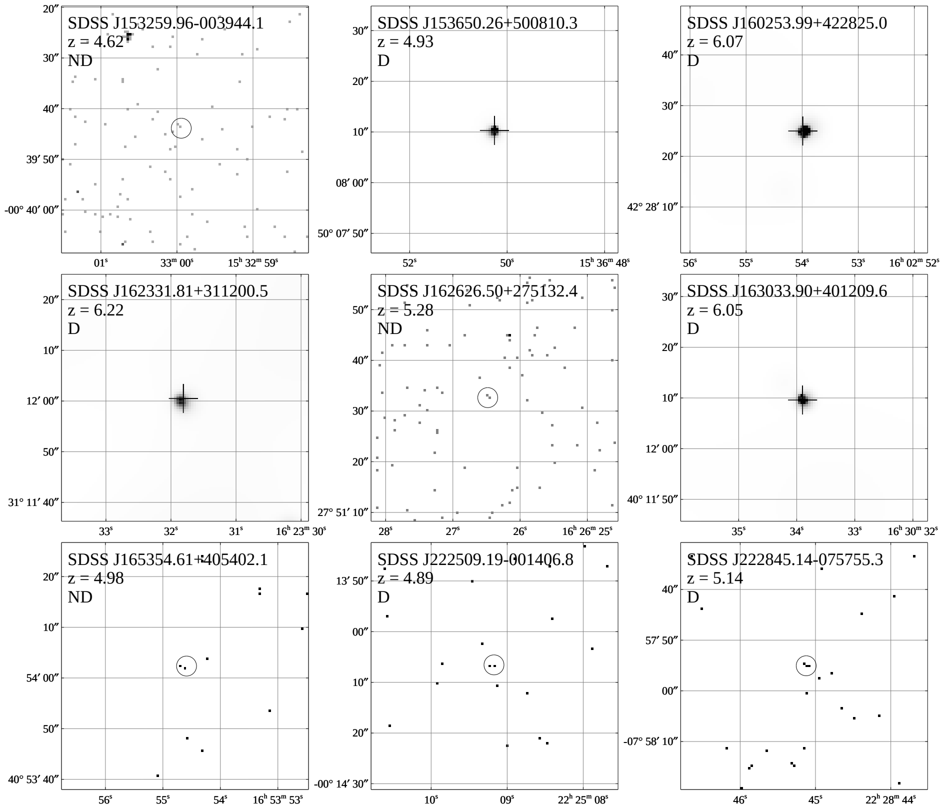

FIG. 2.— *Continued*

One source, SDSS J0011+1446, is a RLQ with $R = 136$, and another source, SDSS J1442+0110, is radio moderate with $R = 32$. Seven sources have upper limits on R that are not tight enough to rule out the possibility that they might be radio moderate.

4. NOTES ON INDIVIDUAL OBJECTS

SDSS J001115.23+144601.8 ($z = 4.97$): This is the only RLQ in our sample ($R = 136$), and it is one of the most X-ray luminous quasars at $z > 4$ with $L_{2-10\,\mathrm{keV}} = 3.2 \times 10^{46}$ erg s^{-1} (cf. Page et al. 2005; Vignali et al. 2003b, 2005). The basic X-ray, optical, and radio properties of the source were first presented in Schneider et al. (2005). The $\Delta\alpha_{\rm ox}(\sigma) = +0.40\,(3.1)$ of the source indicates that it significantly deviates from the $\alpha_{\rm ox}$–$L_\nu(2500\,\mathrm{\AA})$ relation, being brighter by a factor of $\approx$11 in X-rays than RQQs of matched UV luminosity. This suggests that the X-ray emission from the source is jet dominated. The relatively large number ($\approx$127) of photons detected from the source also allowed a basic investigation of its X-ray spectrum, which was extracted with the CIAO task PSEXTRACT using a circular region of $2''$ radius centered on the X-ray centroid. The background region was an annulus with inner and outer radii of $5''$ and $25''$, respectively. The spectrum was binned in groups of 10 counts per bin. We used XSPEC v11.3.2 (Arnaud 1996) to fit the spectrum with a power-law model and a Galactic absorption component (Dickey & Lockman 1990), which was kept fixed during the fit. The spectrum and its best-fit model and residuals appear in Fig. 3. The best-fit photon index is $\Gamma = 1.75^{+0.37}_{-0.35}$ with $\chi^2 = 11.02$ for 9 degrees of freedom (DOF); such a relatively flat power law is typical among RLQs (e.g., Reeves & Turner 2000). Adding an intrinsic absorption component at the redshift of the quasar did not improve the fit, and in particular did not remove the 2σ residuals at $\approx$0.6 and $\approx$1.2 keV. The residuals at $\approx$1.2 keV are consistent in energy with a redshifted Fe Kα line, but we do not expect such a line in a highly beamed and X-ray-luminous source (e.g., Page et al. 2004). The remaining residuals in our spectrum are therefore difficult to interpret and should be investigated with a higher signal-to-noise ratio spectrum.

SDSS J104845.05+463718.3 ($z = 6.19$): This is one of two BALQSOs in our sample. The quasar was discovered by Fan et al. (2003), who detected a hint of a Si IV BAL trough in the optical spectrum of the source. It was later confirmed as a BALQSO by Maiolino et al. (2004), based on its IR spectrum, and it is the most distant BALQSO discovered to date. Millimeter observations of this source detected dust emission and suggested a star-formation rate of $\sim 2000\,M_\odot$ yr^{-1} (Bertoldi et al. 2003). BALQSOs typically show soft X-ray absorption with intrinsic X-ray column densities in the range $N_{\rm H}{\approx}10^{22}$–$10^{24}$ cm^{-2}, rendering them weak X-ray sources (e.g., Gallagher et al. 1999, 2006). Since we have accessed highly penetrating X-rays ($\sim$4–70 keV) from the source, any X-ray flux attenuation due to absorption at the quasar redshift has been mitigated, allowing easier detection. We find that the source has $\alpha_{\rm ox}{=}\,-1.94$, which is consistent with the predicted value for a non-BAL RQQ

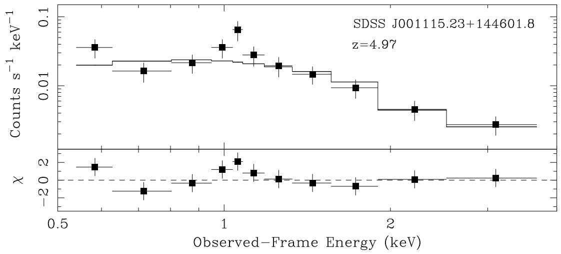

FIG. 3.— *Chandra* spectrum of SDSS J0011+1446. Filled squares represent the binned spectrum, and the solid histogram represents the best-fit power-law model. The χ residuals are in units of σ with error bars of size 1. Note the 2σ residuals at ~ 0.6 keV and ~ 1.2 keV.

with matched UV luminosity ($\alpha_{\rm ox}= -1.72$) at a level of 1.4σ (Table 3). The $\Delta\alpha_{\rm ox}= -0.22$ for the source is also consistent with the mean difference between the absorption-corrected $\alpha_{\rm ox}$ and the predicted $\alpha_{\rm ox}$ values determined for a sample of 35 BALQSOs (see Figure 2 of Gallagher et al. 2006).

SDSS J130216.13+003032.1 ($z = 4.47$): This WLQ was first noted by Anderson et al. (2001) to have weak Lyα emission and an optical spectrum that is similar to the prototype quasar of this class, SDSS J1532−0039 (Fan et al. 1999). We did not detect this source in our *Chandra* observation; the upper limit on its $\alpha_{\rm ox}$, -1.81, is consistent at a level of 1σ with the predicted $\alpha_{\rm ox}$ (Table 3). Thus, the present data cannot prove that this source is anomalously X-ray weak.

SDSS J140850.91+020522.7 ($z = 4.01$): This WLQ was first reported by Schneider et al. (2003). Even though it is one of three quasars in our sample that is radio detected, its radio-to-optical flux ratio, $R = 8.1$, clearly classifies it as radio quiet. It is one of two WLQs that we detect in the X-rays, and its $\alpha_{\rm ox}= -1.54$ is consistent with the predicted value at a level of 1σ (Table 3).

SDSS J144231.72+011055.2 ($z = 4.51$): This WLQ is radio moderate with $R = 32$. It was first presented by Anderson et al. (2001), who noted its similarity to SDSS J1532−0039 (Fan et al. 1999). The source is quite X-ray bright, with $L_{2-10\,{\rm keV}} = 2.5 \times 10^{45}$ erg s^{-1}. The relatively flat $\alpha_{\rm ox}= -1.42$ we find is typical of radio moderate-to-loud quasars, and it is consistent with the predicted $\alpha_{\rm ox}$ for RQQs of matched UV luminosity at a level of 1.4σ (Table 3); this indicates a factor of ~ 4 excess in X-ray flux compared with the predicted RQQ value. The weak emission lines may be due to dilution by a beamed continuum source. The strong X-ray emission may also suggest the presence of a moderately beamed X-ray continuum component, which is in accordance with the fact that it is only moderately strong in the radio.

SDSS J153259.96−003944.1 ($z = 4.62$): This is the prototype high-z WLQ, discovered by Fan et al. (1999), who also found a radio-to-optical spectral index of $\alpha_{\rm ro} > -0.02$[11] for the source; this $\alpha_{\rm ro}$ lower limit is equivalent to $R < 1.0$ (Table 3), making this source a RQQ. By monitoring the source during 2000–2001, Stalin & Srianand (2005) found that it is optically variable, in the R and I bands, at a level of $\approx$0.3 mag; their claim of a ~ 0.9 mag difference between the SDSS photometry obtained in 1998 (Fan et al. 1999)

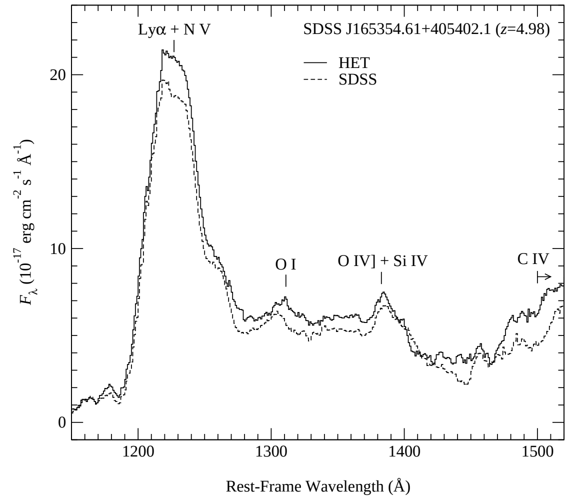

FIG. 4.— HET spectrum of SDSS J1653+4054 (*solid curve*) superposed on the SDSS spectrum of the source (*dashed curve*). Both spectra have been smoothed with a 10 Å boxcar filter. A shallow C IV BAL trough is apparent in both spectra at ~ 1450 Å. The small differences between the two spectra, which are separated by 124 d in the rest-frame, are probably due to systematics of the different instruments and calibration methods used.

and their 2001 photometry of the source was probably a consequence of incorrect magnitude conversions between the SDSS and Cousins magnitude systems. The source was targeted by *Chandra* in Cycle 2 but was undetected in a 5.09 ks observation (Vignali et al. 2001). We targeted this source with *Chandra* again in Cycle 6 and observed it for 9.83 ks. It remains undetected, and the combined exposure time of 14.92 ks yields $\alpha_{\rm ox} < -1.90$, which is consistent with the predicted $\alpha_{\rm ox}$ at a level of 1.5σ (Table 3). An additional *Chandra* exposure of $\approx$60 ks would be required to determine if this source is notably X-ray weak (at a 3σ level).

SDSS J162331.81+311200.5 ($z = 6.22$): Discovered by Fan et al. (2004), this quasar has the strongest Lyα emission line known at $z > 5$; the total rest-frame equivalent width (REW) of Lyα and N V λ1240 is $\gtrsim 150$ Å, compared with a mean REW(Lyα+N V) of 69.3±18.0 Å for $z > 4$ quasars (Fan et al. 2001). Otherwise, this source is not particularly optically luminous; we detected it with *Chandra* and found $\alpha_{\rm ox}= -1.82$, which is consistent with the predicted value at a 1σ level.

SDSS J165354.61+405402.1 ($z = 4.98$): Following the approval of our *Chandra* program, we re-investigated the optical properties of our approved targets. The SDSS spectrum of this source (obtained on 2001 June 19) showed a hint of a C IV BAL trough, which we subsequently confirmed with a 15 minute exposure of the source, on 2003 July 1, using the Marcarian Low-Resolution Spectrograph (Hill et al. 1998) on the 9 m Hobby-Eberly Telescope (HET; Ramsey et al. 1998; see Fig. 4). These spectra suggest that the quasar is a BALQSO with a C IV absorption trough having REW$\simeq 25$ Å and an outflow velocity in the range $1.4 \times 10^4 \lesssim v \lesssim 3.1 \times 10^4$ km s^{-1}. We do not detect this source in our *Chandra* observation, obtaining $\alpha_{\rm ox} < -1.74$, which is consistent with the predicted value for a non-BAL RQQ with matched luminosity at a 0.3σ level (Table 3). The $\Delta\alpha_{\rm ox} < -0.05$ we find is also consistent with the mean difference between the absorption-corrected $\alpha_{\rm ox}$ and the predicted $\alpha_{\rm ox}$ values determined for a sample of 35 BALQSOs (cf. Figure 2 of Gallagher et al. 2006).

[11] We adopt the definition of $\alpha_{\rm ro}$ from Stocke et al. (1990); this is equivalent to the definition of $\alpha_{\rm ox}$ (Eq. 1), where the 2 keV flux density and frequency are replaced by the corresponding values at 5 GHz.

TABLE 4
PROPERTIES OF $z > 5$ RADIO-QUIET QUASARS INCLUDED IN THE JOINT FITTING

Object (SDSS J)	z	$N_{\rm H}$[a]	X-ray Obs. Date	Exp. Time[b] (ks)	Full-Band Total Counts	Ref.
000239.39+255034.8	5.80	4.09	2005 Jan 24	5.87	$5.0^{+3.4}_{-2.2}$	1
000552.34−000655.8	5.85	3.14	2005 Jul 28	16.93	$17.6^{+5.3}_{-4.1}$	1
023137.65−072854.5	5.41	2.90	2002 Sep 27	4.20	$23.9^{+6.0}_{-4.9}$	2
075618.14+410408.6	5.11	4.76	2002 Feb 8	7.33	$14.8^{+4.9}_{-3.8}$	2
083643.85+005453.3[c]	5.77	4.40	2002 Jan 29	5.70	$20.7^{+5.6}_{-4.5}$	3
084035.09+562419.9	5.85	4.37	2005 Feb 3–4	15.84	$3.0^{+2.9}_{-1.6}$	1
103027.10+052455.0	6.28	2.70	2002 Jan 29	8.10	$5.8^{+3.6}_{-2.3}$	3
105322.98+580412.1	5.21	0.56	2001 July 5	4.70	$4.3^{+3.3}_{-2.0}$	1
120441.72−002149.5	5.03	2.12	2000 Dec 2	1.57	$8.0^{+4.0}_{-2.8}$	4
130608.26+035626.3	5.99	2.07	2002 Jan 29	8.20	$16.8^{+5.2}_{-4.1}$	3
141111.29+121737.4	5.93	1.69	2005 Mar 17	14.27	$12.9^{+4.7}_{-3.5}$	1
160253.98+422824.9	6.07	1.33	2005 Oct 29	13.20	$26.3^{+6.2}_{-5.1}$	1
162331.81+311200.5	6.22	2.05	2004 Dec 29	17.21	$5.7^{+3.5}_{-2.3}$	1
163033.90+401209.6	6.05	0.86	2005 Nov 4	27.39	$17.4^{+5.3}_{-4.1}$	1
222845.14−075755.3	5.14	4.67	2003 May 5	7.04	$3.0^{+2.9}_{-1.6}$	1

REFERENCES. — (1) This work; (2) Vignali et al. (2003b); (3) Brandt et al. (2002); (4) Bechtold et al. (2003).

[a]Neutral Galactic absorption column density in units of 10^{20} cm^{-2} taken from Dickey & Lockman (1990).

[b]The *Chandra* exposure time has been corrected for detector dead time.

[c]This source has a radio counterpart in the FIRST catalog, with a flux of 1.11±0.15 mJy at an observed-frame wavelength of 20 cm; given the optical flux of the source, the radio-loudness parameter is $R \lesssim 10$, which ranks this quasar, at most, as radio moderate (e.g., Brandt et al. 2002).

5. X-ray SPECTRAL PROPERTIES OF THE MOST DISTANT QUASARS

Obtaining meaningful X-ray spectral properties, such as the power-law photon index and the intrinsic absorption column density, for the individual sources in this work (with the exception of SDSS J0011+1446) is hindered by the small numbers of detected photons. To date, such measurements have been done for only 10 quasars at $z > 4$ (e.g., Shemmer et al. 2005 and references therein). Our knowledge of the X-ray spectral properties of quasars at $z > 4$ therefore relies mainly on joint spectral fitting of samples of such sources. For example, Vignali et al. (2005) jointly fitted spectra of 48 $z > 4$ RQQs at a mean redshift of 4.3; they found a mean photon index of $\Gamma = 1.93^{+0.10}_{-0.09}$ and have constrained the mean intrinsic neutral absorption column to $N_{\rm H} \lesssim 5\times10^{21}$ cm^{-2}.

We jointly fitted the spectra of all optically selected $z > 5$ RQQs, excluding BALQSOs, which were detected with > 2 and $\lesssim 30$ full-band counts (the maximum limit prevents one or a few sources from dominating the average spectrum). This allows investigation of the mean X-ray spectral properties of the most distant quasars known, shedding light on the X-ray production mechanism and the central environment of quasars at the end of the reionization epoch. Using these criteria we found nine suitable sources from this work and six archival sources, all observed with *Chandra*. Table 4 lists all 15 sources used in the joint fitting process along with the total number of counts detected for each source. The mean (median) redshift of this group of quasars is 5.72 (5.85), with a total of 185 full-band counts, obtained in 158 ks.

The X-ray spectra were extracted with PSEXTRACT using circular regions of 2″ radius centered on the X-ray centroid of each source (except for SDSS J1053+5804, in which a 4″ radius was used due to its off-axis position on the CCD). Although the background is typically negligible in these *Chandra* observations, we have extracted background counts using annuli of different sizes (to avoid contamination from nearby X-ray sources) centered on each source. We used XSPEC V11.3.2 (Arnaud 1996) to fit the set of 15 unbinned spectra jointly with the following models: (i) a power-law model and a Galactic absorption component (Dickey & Lockman 1990), which was kept fixed during the fit, and (ii) a model similar to the first with an added intrinsic (redshifted) neutral-absorption component. All fits assumed solar abundances (Anders & Grevesse 1989; Dietrich et al. 2003), used the PHABS absorption model in XSPEC with the Balucinska-Church & McCammon (1992) cross-sections, and used the C-statistic (Cash 1979); this statistical approach allows one to retain all spectral information and to associate with each quasar its own Galactic absorption column density and redshift. The errors associated with the best-fit X-ray spectral parameters are quoted at the 90% confidence level for one parameter of interest ($\Delta C = 2.71$; Avni 1976; Cash 1979).

The joint-fitting process was carried out three times for both models. In the first run, we included the entire observed-energy range of all the spectra (0.5–8 keV). In the second run we included only the common rest-frame energy range of all 15 sources: $3.64 \lesssim E_{\rm rest} \lesssim 48.24$ keV (corresponding to 0.5–8 keV in the observed frame). In the third run we fitted the entire observed-energy range of ten (out of 15) quasars with $z > 5.5$ (the common rest-frame energy range for these quasars is almost identical to the entire observed-energy range due to their very narrow redshift distribution). Table 5 lists the best-fit parameters from the joint-fitting process, and a contour plot of the Γ-$N_{\rm H}$ parameter space is shown in Fig. 5. We find that, in the case of the entire energy range, the mean X-ray power-law photon index of $z > 5$ RQQs is $\Gamma = 1.95^{+0.30}_{-0.26}$, and their mean neutral intrinsic absorption column density is $N_{\rm H} \lesssim 6\times10^{22}$ cm^{-2}. These results are consistent with those based on the common energy range and on the

TABLE 5
BEST-FIT PARAMETERS FROM JOINT FITTING OF $z > 5$ RADIO-QUIET QUASARS

Spectral Model Galactic-Absorbed Power-Law and	Number of Sources	Mean (Median) Redshift	Energy Range[a]	N_H (10^{22} cm^{-2})	Γ	*C*-statistic (bins)
...	15	5.72 (5.85)	E	...	$1.95^{+0.27}_{-0.26}$	158.6 (175)
...	15	5.72 (5.85)	C	...	$1.97^{+0.29}_{-0.28}$	154.8 (168)
...	10	5.98 (5.96)	E	...	$1.98^{+0.31}_{-0.32}$	121.2 (124)
Intrinsic Absorption	15	5.72 (5.85)	E	≤ 5.98	$1.95^{+0.30}_{-0.26}$	158.6 (175)
Intrinsic Absorption	15	5.72 (5.85)	C	≤ 6.63	$1.97^{+0.30}_{-0.28}$	154.8 (168)
Intrinsic Absorption	10	5.98 (5.96)	E	≤ 8.64	$1.98^{+0.37}_{-0.32}$	121.2 (124)

NOTE. — The joint fitting process was carried out three times for each model. In the first run we fitted the entire energy range of all $z > 5$ quasars, and in the second run we fitted their spectra in their common energy range. In the third run we fitted the spectra of 10 $z > 5.5$ quasars in their entire energy range.

[a]E - entire energy range of all the spectra. C - the common rest-frame energy range among all sources (3.64–48.24 keV).

sub-group of $z > 5.5$ quasars due to the relatively narrow redshift range of the sample and the fact that most of the quasars are at $z > 5.5$.

The mean power-law photon index of optically selected $z > 5$ RQQs is consistent with the mean photon index, $\Gamma = 1.93^{+0.10}_{-0.09}$, obtained by jointly fitting spectra of 48 RQQs at $\langle z \rangle = 4.3$ (Vignali et al. 2005), and with the mean photon index, $\Gamma = 1.97^{+0.06}_{-0.04}$, obtained by jointly fitting high-quality spectra of eight RQQs at $\langle z \rangle = 4.8$ (Shemmer et al. 2005). The mean photon index we obtain for $z > 5$ RQQs is also consistent with photon-index measurements for individual RQQs at lower redshifts (e.g., Reeves & Turner 2000; Vignali et al. 2001; Page et al. 2005; Piconcelli et al. 2005). Even though the upper limit we obtained on the mean neutral intrinsic absorption column in $z > 5$ RQQs, $N_H \lesssim 6 \times 10^{22}$ cm^{-2}, is about an order of magnitude weaker than previous N_H upper limits obtained for $z > 4$ RQQs with similar methods ($N_H \lesssim 5 \times 10^{21}$ cm^{-2} at $\langle z \rangle = 4.3$; Vignali et al. 2005; $N_H \lesssim 3 \times 10^{21}$ cm^{-2} at $\langle z \rangle = 4.8$; Shemmer et al. 2005), it implies that RQQs were not heavily absorbed when the age of the Universe was $\lesssim 1$ Gyr.

We have plotted α_{ox} for all the RQQs in our sample against their UV luminosity in Figure 6, and included all 333 RQQs from the Steffen et al. (2006) study in this diagram. Our sources, which comprise most of the highest-redshift quasars known, follow the correlation between α_{ox} and UV luminosity with no detectable dependence on redshift. Figure 7 shows the α_{ox} distribution of 21 optically selected $z > 5$ quasars (11 sources from this work and 10 from the literature) and the $\Delta\alpha_{ox}$ distribution given their UV luminosities. We also calculated the mean α_{ox} of the 18 non-BAL RQQs in that sample using the ASURV software package (Lavalley, Isobe, & Feigelson 1992) to account for two α_{ox} upper limits, and found $\langle \alpha_{ox} \rangle = -1.69 \pm 0.03$ (where the quoted error is the error on the mean). This value is consistent with the mean α_{ox} predicted from the Steffen et al. (2006) relation, $\langle \alpha_{ox} \rangle = -1.68 \pm 0.15$ (where the quoted error is the standard deviation), given the mean UV luminosity of the sources. The $\Delta\alpha_{ox}$ distribution of $z > 5$ quasars indicates that α_{ox} values for most of the sources are consistent within $\pm 1\sigma$ with the predicted values, and none of the sources is significantly X-ray weak (Fig. 7b). Our results strongly support the idea that AGN SEDs have not significantly evolved out to the highest observable redshifts.

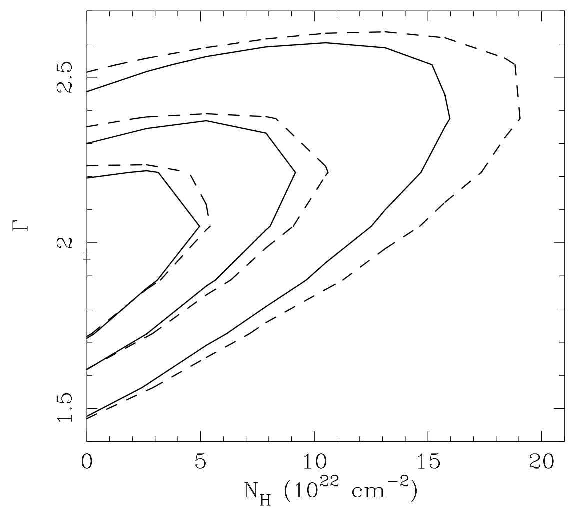

FIG. 5.— 68%, 90%, and 99% confidence regions for the photon index vs. intrinsic column density derived from joint spectral fitting of our sample of 15 RQQs at $z > 5$. Solid (dashed) contours refer to the entire (common) energy range of the quasars (see § 5 for more details). Note that the markers for the best fit parameters in each fit lie on the vertical axis.

6. X-RAY CLUES TO THE NATURE OF WEAK EMISSION-LINE QUASARS

We have observed four members of the rare class of WLQs with *Chandra*. Three of these sources are radio quiet, and one, SDSS J1442+0110, is radio moderate. SDSS J1408+0205 and SDSS J1442+0110 are the only X-ray-detected WLQs in our sample, and their α_{ox} values, -1.54 and -1.42, respectively, appear relatively flat although not exceptional (Table 3). Both of these sources are also radio detected, although SDSS J1408+0205 is, by definition, a RQQ (R=8.1). SDSS J004054.65−091526.8 (z=4.98) is another radio-quiet X-ray-detected WLQ; it was serendipitously detected in an *XMM-Newton* observation of the galaxy cluster Abell 85, and its basic X-ray properties are presented in Schneider et al. (2003) who found α_{ox}=-1.55. Our data are therefore suggestive of two groups of WLQs: (i) radio-quiet WLQs that are also X-ray weak, including SDSS J1302+0030 and SDSS J1532−0039, and (ii) WLQs that are mildly X-ray bright, with a relatively flat α_{ox}. The second group includes

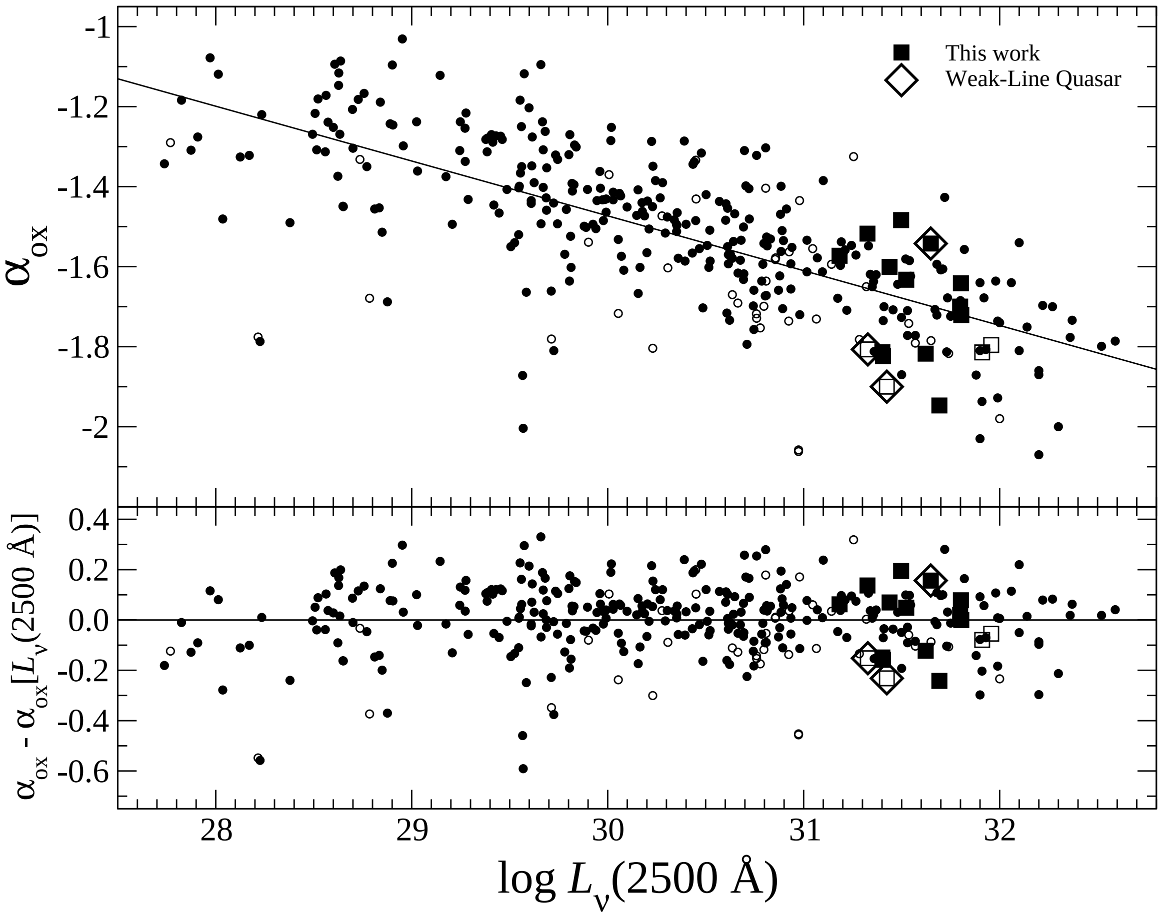

FIG. 6.— The α_{ox}–L_ν(2500 Å) relationship for RQQs, excluding known BALQSOs, adapted from Steffen et al. (2006). Open symbols indicate α_{ox} upper limits. Our sources are marked with squares, and enclosing diamonds mark the radio-quiet WLQs in our sample (note that the radio-moderate WLQ, SDSS J1442+0110, is not included in the diagram). The Steffen et al. (2006) best-fit line is shown in the top panel, and the bottom panel shows the α_{ox} residuals ($\Delta\alpha_{ox}$) from that best-fit line.

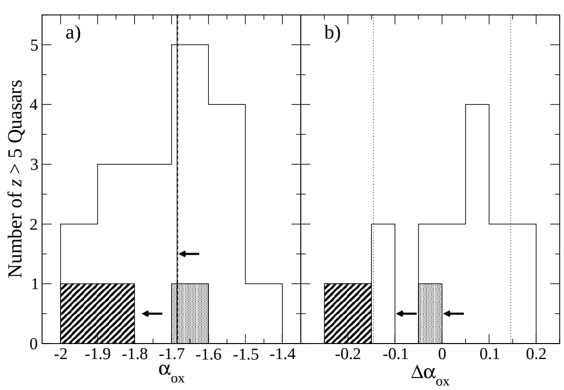

FIG. 7.— Histograms of (*a*) α_{ox} and (*b*) $\Delta\alpha_{ox}$ for all optically selected $z > 5$ quasars from this work and the literature. Radio-loud quasars are shaded, and BALQSOs are hatched. Upper limits are marked by arrows. The solid (dashed) line in panel (*a*) marks the mean measured (predicted) α_{ox} of optically selected $z > 5$ RQQs, excluding the BALQSOs (note that the two lines almost overlap). Dotted lines in panel (*b*) mark the 1σ range ($\sigma = \pm 0.146$) for the distribution of $\Delta\alpha_{ox}$ for sources with $31 < \log L_\nu(2500\,\text{Å}) < 32$ from Steffen et al. (2006).

the two WLQs with radio detections (although these are not RLQs), SDSS J1408+0205 and SDSS J1442+0110, and the radio-undetected source SDSS J0040−0915.

Since the discovery of the prototype WLQ, SDSS J1532−0039 (Fan et al. 1999), about a dozen WLQs have been discovered at $z > 2$ with REW(Lyα)< 5 Å (Anderson et al. 2001; Schneider et al. 2003, 2005; Collinge et al. 2005; Fan et al. 2006). We are also aware of at least two quasars at lower redshifts that lack high-ionization emission lines in their spectra, and whose optical luminosities are comparable to those of our WLQs; these are PG 1407+265 (z=0.94; McDowell et al. 1995) and PHL 1811 (z=0.19; Leighly et al. 2001) that may also be members of the WLQ class (see also Hawkins 2004). In contrast with their lack of Lyα and high-ionization lines, PG 1407+265 and PHL 1811 exhibit a strong and broad Hα and Hβ emission line, respectively. Another possible member of the WLQ class, 2QZ J215454.3−305654 at z=0.494, shows only an [O III] λ5007 emission line, but since UV spectroscopy of the source was not yet carried out, it is unknown whether it displays higher ionization lines (Londish et al. 2004).

6.1. *Boosted Continuum vs. Depleted High-Ionization Gas*

Some of the plausible explanations for the weakness, or absence, of high-ionization broad emission lines in WLQs include abnormal photoionizing continuum or broad emission line region (BELR) properties, and a low BELR covering factor. For example, such quasars may have a deficit of line-emitting gas in the vicinity of the central continuum source since an accretion-disk wind, proposed as a production site for some of the BELR lines (e.g., Murray & Chiang 1997), may not form, perhaps due to exceptionally high Eddington ratios (e.g., Leighly, Halpern, & Jenkins 2004), but see also Nicastro

(2000). As a result of the high accretion rate, the continuum is expected to be correspondingly softer, thus suppressing high-ionization emission lines, but having little effect on the low-ionization species. A softer (X-ray) and bluer (UV–optical) continuum, as well as Hβ and Fe II blends are indeed observed in PHL 1811 (Leighly et al. 2004), although PG 1407+265 displays a 'normal' quasar continuum (McDowell et al. 1995).

Many featureless-spectrum AGNs are identified as BL Lacertae objects (hereafter BL Lacs) whose emission lines are diluted by relativistic beaming of their optical continua (e.g., Urry & Padovani 1995). Based on their weak-lined spectra alone, a BL Lac classification is another plausible explanation for the nature of WLQs. Most BL Lacs are low-to-moderate luminosity AGNs, discovered at $z \lesssim 1$ (e.g., Perlman et al. 2001 and references therein). By virtue of their weak-line spectra, the redshifts of BL Lacs are difficult to obtain and can be highly uncertain. Collinge et al. (2005) have found that BL Lac candidates with no significant proper motions and with either radio or X-ray detections tend to lie in specific regions of SDSS optical color-color diagrams. In particular, their $z < 1$ BL Lac candidates have optical colors that are significantly redder than those of typical quasars. All of our WLQs have relatively accurate redshift measurements due to a clear Lyman-break feature, and their optical spectra resemble those of six of the Collinge et al. (2005) BL Lac candidates at $z > 2.15$ (the redshift threshold where Lyα enters the SDSS spectra).

Most known BL Lacs are strong radio and X-ray sources (relative to their optical emission), but the radio/X-ray-weak region in the BL Lac $\alpha_{\rm ro}$–$\alpha_{\rm ox}$ "color-color" diagram is being increasingly populated by deep radio and X-ray surveys (e.g., Perlman et al. 2001 and references therein). In Figure 8 we plot the $\alpha_{\rm ro}$–$\alpha_{\rm ox}$ diagram for all the BL Lacs from Perlman et al. (2001) and E. Perlman (2006), private communication; we also add to the plot the $z > 2.15$ BL Lac candidates from Collinge et al. (2005), the three $z < 1$ WLQs (2QZ J2154$-$3056, PG 1407+265, and PHL 1811), and the five $z > 4$ WLQs discussed in this work. The region occupied by typical radio-quiet AGNs is also marked in Fig. 8 (compare with Fig. 6). Apparently, the two radio- and X-ray-detected $z > 4$ WLQs (from our second group of WLQs), SDSS J1408+0205 and SDSS J1442+0110, are similar to (X-ray selected) radio-weak BL Lacs. The two radio- and X-ray-undetected $z > 4$ WLQs (from our second group of WLQs) and PHL 1811 might appear to constitute the tail of the radio/X-ray-weak BL Lac population, but their radio and X-ray properties are also consistent with those of typical RQQs. According to Fig. 8, most of the $z > 2.15$ BL Lac candidates from Collinge et al. (2005) are consistent with the radio and X-ray properties of both radio-weak BL Lacs and typical RQQs, although the loose constraints on their $\alpha_{\rm ox}$ values (based on *ROSAT* measurements) prevent a proper distinction between BL Lacs and RQQs, as well as a comparison with the WLQs.

Since most BL Lacs at $z \lesssim 1$ are strong radio sources, it is interesting to note that most WLQs, and the Collinge et al. (2005) $z > 2.15$ BL Lac candidates, are radio weak. The lack of radio-loud ($\alpha_{\rm ro} < -0.4$, equivalent to $R > 100$) WLQs might perhaps be attributed to the fact that they are all highly optically luminous sources. We investigated this possibility by examining the luminosities, $\alpha_{\rm ro}$, and $\alpha_{\rm ox}$ values of samples of lower-redshift ($z \lesssim 1$) BL Lacs. While BL Lacs from the EMSS sample (e.g., Rector et al. 2000) tend to be more radio/X-ray-weak at high optical luminosities, the BL Lacs from the larger RGB sample (Laurent-Muehleisen et al. 1999) do not show this trend, and weak (and strong) radio sources are found at all luminosities. However, this is not sufficient to rule out a possible luminosity effect, since even the most luminous BL Lacs considered are two orders of magnitude less optically luminous than our WLQs, thus preventing a straightforward comparison of the radio properties between the two classes of sources. The lack of highly optically luminous BL Lacs may be a consequence of their selection, which is performed mainly with radio and X-ray surveys. Since it is possible that these selection methods have allowed highly optically luminous BL Lacs to escape detection, we checked for a radio-loudness–luminosity relation among the Collinge et al. (2005) optically-selected sample of low-redshift BL Lac candidates, but no clear trend has been found.

Two other well-known characteristics of BL Lacs are rapid and large-amplitude optical flux variations, and high levels (up to 40%) of optical polarization (e.g., Jannuzi, Smith, & Elston 1994). Stalin & Srianand (2005) have detected optical flux variations at a level of ≈ 0.3 mag in the prototype WLQ, SDSS J1532$-$0039, on an observed-frame time baseline of 450 d (80 d in the rest-frame), although this is somewhat lower than, and not as fast as, the level displayed by typical BL Lacs (e.g., Ghosh et al. 2000). Fan et al. (1999) have constrained the optical polarization level of SDSS J1532$-$0039 to be $\leq 4\%$. This is consistent with single-epoch measurements of polarization levels in X-ray-selected BL Lacs, which are typically lower than the polarization levels observed in radio-selected BL Lacs (e.g., Jannuzi et al. 1994; Visvanathan & Wills 1998). Therefore, low optical polarization levels in WLQs might be expected due to their radio weakness, regardless of whether they are BL Lacs or not.

While the nature of WLQs remains mysterious and apparently there is significant variety among this class of sources, a 'boosted continuum' or a 'suppression of high-ionization BELR lines' remain the most likely scenarios. The significant overlap in the radio and X-ray properties between different AGN classes (i.e., BL Lacs and radio-quiet AGNs) as well as the multiple selection biases, as depicted in the $\alpha_{\rm ro}$–$\alpha_{\rm ox}$ diagram (Fig. 8), might cause physically distinct AGN populations to blend together, and thus prevent a clear conclusion for the nature of WLQs. This calls for a more thorough and systematic investigation of the 'continuum boosting' versus 'high-ionization emission-line suppression' scenarios via more observations such as those described below, and detailed photoionization modeling. While relativistic boosting of the continuum may be consistent with the optical spectra, radio fluxes, and X-ray fluxes of the sources from our second group of WLQs as well as with some of the $z > 2.15$ BL Lac candidates of Collinge et al. (2005), it cannot hold for the two $z < 1$ WLQs that display Balmer emission lines. It is also hard to accept a boosting scenario for our first group of WLQs and most of the $z > 2.15$ BL Lac candidates of Collinge et al. (2005), due to the weakness of their radio and X-ray emission. In addition, the fact that radio-loud WLQs (with $R > 100$) are missing is naturally explained by the 'line suppression' scenario, which does not require that the quasars be radio-loud. The following observations for all $z > 4$ WLQs and the $z > 2.15$ BL Lac candidates of Collinge et al. (2005) are required to enable a clearer distinction between the two proposed scenarios:

1. Sensitive near-IR spectroscopy to reveal any low-ionization emission lines (e.g., Balmer or Fe II lines)

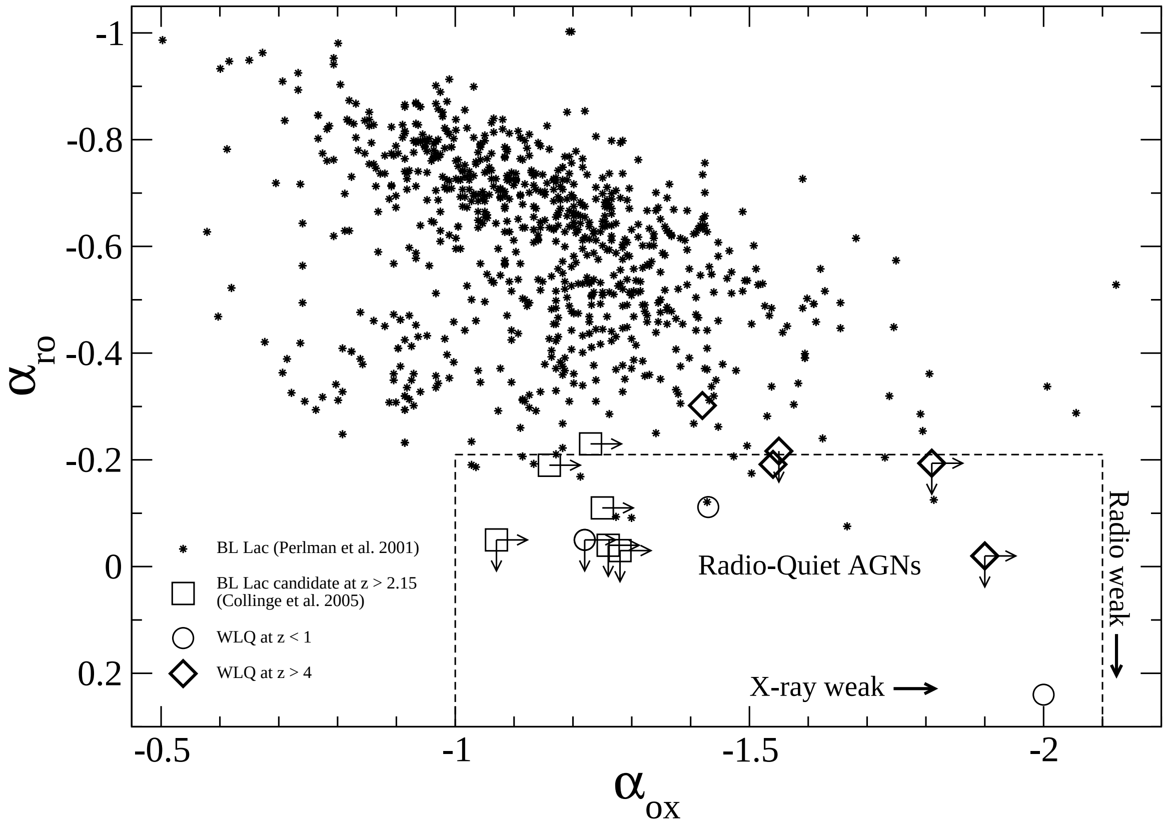

FIG. 8.— The α_{ro}–α_{ox} diagram for BL Lacs, adapted from Perlman et al. (2001). Stars mark BL Lacs selected from radio and X-ray surveys (Perlman et al. 2001, and E. Perlman 2006, private communication). Squares mark $z > 2.15$ BL Lac candidates from Collinge et al. (2005), circles mark the $z < 1$ WLQs (2QZ J2154−3056, PG 1407+265 and PHL 1811; the first of these sources is not detected in both radio and X-rays, and the latter is the radio-weakest source on this diagram), and diamonds mark $z > 4$ WLQs. Right (down) pointing arrows mark α_{ox} (α_{ro}) upper limits. Dashed lines mark the region containing most radio-quiet AGNs. Note that the WLQs and $z > 2.15$ BL Lac candidates lie among known radio-weak BL Lacs, and that most sources from these three groups overlap with radio-quiet AGNs.

and determine whether the UV–optical continua are typical of RQQs. Clear detection of low-ionization lines, and/or a typical (or bluer) continuum will support the 'high-ionization line suppression' scenario, while the non-detection of such lines and redder continua will support the BL Lac interpretation.

2. *Spitzer* near–mid-IR observations (using *IRAC* and *MIPS*) may determine whether the SED is consistent with a typical AGN IR 'bump' or with a beamed, 'bump-less', continuum.

3. Optical–near-IR photometric monitoring to detect rapid and large-amplitude flux variations can check for a boosted continuum.

6.2. *A Macro- or Micro-Lensing Interpretation?*

The absence of prominent optical emission lines in luminous, high-redshift quasars has raised several other possible explanations for their peculiar spectra. One of these is that high-redshift WLQs are not quasars at all, but rather normal galaxies (e.g., Ivison et al. 2005). Their measured luminosities are much larger than even the most luminous galaxies, but could perhaps be explained by magnification due to gravitational lensing. Our X-ray observations rule out that possibility, at least for the cases of the three X-ray-detected high-redshift WLQs that show AGN-like X-ray properties, i.e., typical AGN optical-to-X-ray flux ratios (see the α_{ox} values in Table 3 and in Schneider et al. 2003; normal galaxies typically have $\alpha_{ox} \ll -2$).

Another possibility is that the continuum source in high-redshift WLQs is amplified relative to the emission from the, much larger, broad emission-line region by gravitational microlensing, since the degree of amplification is inversely proportional to the size of the emitting region (e.g., Paczynski 1986; Schneider & Weiss 1987; Ostriker & Vietri 1990). Such microlensing events are expected to be both relatively short (months–years) and rare, and they might perhaps qualitatively explain the rarity of high-redshift WLQs among the quasar population (e.g., Wambsganss, Schneider, & Paczynski 1990). Testing this scenario would require spectroscopic monitoring of our high-redshift WLQs to search for the reappearance of the emission lines. However, the SDSS images of our WLQs, and the X-ray images of our X-ray-detected WLQs, do not show evidence for multiple images or lensing galaxies in their vicinity, and therefore a microlensing interpretation is unlikely (we also note that our WLQs were not targeted with the *Hubble Space Telescope* by Richards et al. 2006).

7. SUMMARY

We present new *Chandra* observations of 21 $z > 4$ quasars, including most of the highest-redshift quasars known as well as four members of the WLQ class. We have doubled the number of X-ray-detected quasars at $z > 5$, allowing investigation of the X-ray spectral properties of AGNs at the end of the reionization epoch. Our main results can be summarized

as follows:

1. The mean power-law X-ray photon index of $z > 5$ RQQs is Γ=$1.95^{+0.30}_{-0.26}$, and it is consistent with photon indices observed for RQQ samples at lower redshifts.

2. The upper limit on the mean intrinsic-absorption column density of $z > 5$ RQQs is $N_{\rm H} \lesssim 6\times10^{22}$ cm^{-2}, implying that RQQs at the dawn of the modern Universe were not heavily absorbed.

3. The $\alpha_{\rm ox}$ values for individual RQQs in our sample, as well as the mean $\alpha_{\rm ox}$ of $z > 5$ RQQs, excluding BALQSOs, are consistent with the values predicted from their UV luminosities. This strengthens previous findings that AGN SEDs have not significantly evolved over cosmic time.

4. We detected two of our $z > 4$ WLQs in X-rays, and distinguished two types of WLQs: radio-quiet WLQs which are also X-ray weak, and radio-quiet–moderate WLQs (i.e., with $R < 100$) that are mildly X-ray bright. Based on single-epoch optical spectra as well as X-ray and radio fluxes of these sources, we discuss several possible interpretations for the weakness of the broad-emission lines, and in particular, continuum boosting versus high-ionization emission-line suppression, which are the more likely scenarios. We propose sensitive near-IR spectroscopy, near–mid-IR photometry, and optical–near-IR monitoring to disentangle these two scenarios.

We gratefully acknowledge the financial support of *Chandra* X-ray Center grants GO3-4117X and GO5-6094X (O. S., W. N. B., D. P. S), NASA LTSA grant NAG5-13035 (O. S., W. N. B., D. P. S.), and NSF grants AST-0307582 (D. P. S.), AST-0307384 (X. F.), and AST-0307409 (M. A. S.). We thank Pat Hall, Aaron Steffen, and Iskra Strateva for helpful comments and discussions, and Linhua Jiang for obtaining the photometric data for SDSS J0005−0006. We also thank Eric Perlman for kindly providing the $\alpha_{\rm ro}$ and $\alpha_{\rm ox}$ data for Fig. 8. An anonymous referee is gratefully acknowledged for a prompt and constructive report that helped to improve the manuscript. Funding for the creation and distribution of the SDSS Archive has been provided by the Alfred P. Sloan Foundation, the Participating Institutions, the National Aeronautics and Space Administration, the National Science Foundation, the U.S. Department of Energy, the Japanese Monbukagakusho, and the Max Planck Society. The SDSS Web site is http://www.sdss.org/. The SDSS is managed by the Astrophysical Research Consortium (ARC) for the Participating Institutions. The Participating Institutions are The University of Chicago, Fermilab, the Institute for Advanced Study, the Japan Participation Group, The Johns Hopkins University, the Korean Scientist Group, Los Alamos National Laboratory, the Max-Planck-Institute for Astronomy (MPIA), the Max-Planck-Institute for Astrophysics (MPA), New Mexico State University, University of Pittsburgh, University of Portsmouth, Princeton University, the United States Naval Observatory, and the University of Washington. The HET is a joint project of the University of Texas at Austin, the Pennsylvania State University, Stanford University, Ludwig-Maximillians-Universität München, and Georg-August-Universität Göttingen. The HET is named in honor of its principal benefactors, William P. Hobby and Robert E. Eberly. This research has made use of the NASA/IPAC Extragalactic Database (NED) which is operated by the Jet Propulsion Laboratory, California Institute of Technology, under contract with the National Aeronautics and Space Administration.

REFERENCES

Adelman-McCarthy, J. K., et al. 2006, ApJS, 162, 38
Anders, E., & Grevesse, N. 1989, Geochim. Cosmochim. Acta, 53, 197
Anderson, S. F., et al. 2001, AJ, 122, 503
Arnaud, K. A. 1996, ASP Conf. Ser. 101: Astronomical Data Analysis Software and Systems V, 101, 17
Avni, Y. 1976, ApJ, 210, 642
Balucinska-Church, M., & McCammon, D. 1992, ApJ, 400, 699
Barger, A. J., Cowie, L. L., Brandt, W. N., Capak, P., Garmire, G. P., Hornschemeier, A. E., Steffen, A. T., & Wehner, E. H. 2002, AJ, 124, 1839
Bassett, L. C., Brandt, W. N., Schneider, D. P., Vignali, C., Chartas, G., & Garmire, G. P. 2004, AJ, 128, 523
Bauer, F. E., Alexander, D. M., Brandt, W. N., Schneider, D. P., Treister, E., Hornschemeier, A. E., & Garmire, G. P. 2004, AJ, 128, 2048
Bechtold, J., et al. 2003, ApJ, 588, 119
Becker, R. H., White, R. L., & Helfand, D. J. 1995, ApJ, 450, 559
Bertoldi, F., Carilli, C. L., Cox, P., Fan, X., Strauss, M. A., Beelen, A., Omont, A., & Zylka, R. 2003, A&A, 406, L55
Brandt, W. N., Guainazzi, M., Kaspi, S., Fan, X., Schneider, D. P., Strauss, M. A., Clavel, J., & Gunn, J. E. 2001, AJ, 121, 591
Brandt, W. N., et al. 2002, ApJ, 569, L5
Carilli, C. L., et al. 2001, ApJ, 555, 625
Cash, W. 1979, ApJ, 228, 939
Collinge, M. J., et al. 2005, AJ, 129, 2542
Condon, J. J., Cotton, W. D., Greisen, E. W., Yin, Q. F., Perley, R. A., Taylor, G. B., & Broderick, J. J. 1998, AJ, 115, 1693
Dai, X., Chartas, G., Eracleous, M., & Garmire, G. P. 2004, ApJ, 605, 45
Dickey, J. M., & Lockman, F. J. 1990, ARA&A, 28, 215
Dietrich, M., Hamann, F., Shields, J. C., Constantin, A., Heidt, J., Jäger, K., Vestergaard, M., & Wagner, S. J. 2003, ApJ, 589, 722
Eadie, W. T., Dryard, D., James, F. E., Roos, M., & Sadoulet, B. 1971, Statistical Methods in Experimental Physics, (Amsterdam: North-Holland)
Ebeling, H., White, D. A., & Rangarajan, F. V. N. 2006, MNRAS, in press (astro-ph/0601306)
Fan, X., et al. 1999, ApJ, 526, L57
Fan, X., et al. 2001, AJ, 121, 54
Fan, X., et al. 2003, AJ, 125, 1649
Fan, X., et al. 2004, AJ, 128, 515
Fan, X., et al. 2006, AJ, in press (astro-ph/0512080)
Farrah, D., Priddey, R., Wilman, R., Haehnelt, M., & McMahon, R. 2004, ApJ, 611, L13
Freeman, P. E., Kashyap, V., Rosner, R., & Lamb, D. Q. 2002, ApJS, 138, 185
Gallagher, S. C., Brandt, W. N., Sambruna, R. M., Mathur, S., & Yamasaki, N. 1999, ApJ, 519, 549
Gallagher, S. C., Brandt, W. N., Chartas, G., Priddey, R., Garmire, G. P., & Sambruna, R. M. 2006, ApJ, submitted
Garmire, G. P., Bautz, M. W., Ford, P. G., Nousek, J. A., & Ricker, G. R. 2003, Proc. SPIE, 4851, 28
Gehrels, N. 1986, ApJ, 303, 336
Ghosh, K. K., Ramsey, B. D., Sadun, A. C., & Soundararajaperumal, S. 2000, ApJS, 127, 11
Grupe, D., Mathur, S., Wilkes, B., & Osmer, P. 2006, AJ, 131, 55
Hawkins, M. R. S. 2004, A&A, 424, 519
Hill, G. J., Nicklas, H. E., MacQueen, P. J., Tejada, C., Cobos Duenas, F. J., & Mitsch, W. 1998, Proc. SPIE, 3355, 375
Ivison, R. J., Smail, I., Bentz, M., Stevens, J. A., Menéndez-Delmestre, K., Chapman, S. C., & Blain, A. W. 2005, MNRAS, 362, 535
Jannuzi, B. T., Smith, P. S., & Elston, R. 1994, ApJ, 428, 130
Jiang, L., et al. 2006, AJ, submitted
Kaspi, S., Brandt, W. N., & Schneider, D. P. 2000, AJ, 119, 2031
Kellermann, K. I., Sramek, R., Schmidt, M., Shaffer, D. B., & Green, R. 1989, AJ, 98, 1195
Kraft, R. P., Burrows, D. N., & Nousek, J. A. 1991, ApJ, 374, 344
Laurent-Muehleisen, S. A., Kollgaard, R. I., Feigelson, E. D., Brinkmann, W., & Siebert, J. 1999, ApJ, 525, 127
Lavalley, M., Isobe, T., & Feigelson, E. 1992, ASP Conf. Ser. 25: Astronomical Data Analysis Software and Systems I, 25, 245
Leighly, K. M., Halpern, J. P., Helfand, D. J., Becker, R. H., & Impey, C. D. 2001, AJ, 121, 2889
Leighly, K., Halpern, J., & Jenkins, E. 2004, ASP Conf. Ser. 311: AGN Physics with the Sloan Digital Sky Survey, 311, 277
Loeb, A., & Barkana, R. 2001, ARA&A, 39, 19

Londish, D., Heidt, J., Boyle, B. J., Croom, S. M., & Kedziora-Chudczer, L. 2004, MNRAS, 352, 903
Lyons, L. 1991, Data Analysis for Physical Science Students (Cambridge: Cambridge Univ. Press)
Mahabal, A., Stern, D., Bogosavljević, M., Djorgovski, S. G., & Thompson, D. 2005, ApJ, 634, L9
Maiolino, R., Oliva, E., Ghinassi, F., Pedani, M., Mannucci, F., Mujica, R., & Juarez, Y. 2004, A&A, 420, 889
Mathur, S., Wilkes, B. J., & Ghosh, H. 2002, ApJ, 570, L5
McDowell, J. C., Canizares, C., Elvis, M., Lawrence, A., Markoff, S., Mathur, S., & Wilkes, B. J. 1995, ApJ, 450, 585
Murray, N., & Chiang, J. 1997, ApJ, 474, 91
Nicastro, F. 2000, ApJ, 530, L65
Oke, J. B., & Gunn, J. E. 1983, ApJ, 266, 713
Ostriker, J. P., & Vietri, M. 1990, Nature, 344, 45
Paczynski, B. 1986, ApJ, 301, 503
Page, K. L., O'Brien, P. T., Reeves, J. N., & Turner, M. J. L. 2004, MNRAS, 347, 316
Page, K. L., Reeves, J. N., O'Brien, P. T., & Turner, M. J. L. 2005, MNRAS, 364, 195
Pentericci, L., et al. 2003, A&A, 410, 75
Perlman, E. S., Padovani, P., Landt, H., Stocke, J. T., Costamante, L., Rector, T., Giommi, P., & Schachter, J. F. 2001, ASP Conf. Ser. 227: Blazar Demographics and Physics, 227, 200
Petric, A. O., Carilli, C. L., Bertoldi, F., Fan, X., Cox, P., Strauss, M. A., Omont, A., & Schneider, D. P. 2003, AJ, 126, 15
Ramsey, L. W., et al. 1998, Proc. SPIE, 3352, 34
Rector, T. A., Stocke, J. T., Perlman, E. S., Morris, S. L., & Gioia, I. M. 2000, AJ, 120, 1626
Richards, G. T., et al. 2002, AJ, 123, 2945
Richards, G. T., et al. 2004, ApJS, 155, 257
Richards, G. T. et al. 2006, AJ, 131, 49
Schlegel, D. J., Finkbeiner, D. P., & Davis, M. 1998, ApJ, 500, 525
Schneider, P., & Weiss, A. 1987, A&A, 171, 49
Schneider, D. P., Schmidt, M., & Gunn, J. E. 1991, AJ, 101, 2004
Schneider, D. P., et al. 2003, AJ, 126, 2579
Schneider, D. P., et al. 2005, AJ, 130, 367
Schwartz, D. A. 2002, ApJ, 571, L71
Schwartz, D. A., & Virani, S. N. 2004, ApJ, 615, L21
Shemmer, O., Brandt, W. N., Vignali, C., Schneider, D. P., Fan, X., Richards, G. T., & Strauss, M. A. 2005, ApJ, 630, 729
Spergel, D. N., et al. 2003, ApJS, 148, 175
Stalin, C. S., & Srianand, R. 2005, MNRAS, 359, 1022
Steffen, A. T., Barger, A. J., Capak, P., Cowie, L. L., Mushotzky, R. F., & Yang, Y. 2004, AJ, 128, 1483
Steffen, A. T., Strateva, I., Brandt, W. N., Alexander, D. M., Koekemoer, A. M., Lehmer, B. D., Schneider, D. P., & Vignali, C. 2006, AJ, in press
Stern, D., Djorgovski, S. G., Perley, R. A., de Carvalho, R. R., & Wall, J. V. 2000, AJ, 119, 1526
Stocke, J. T., Morris, S. L., Gioia, I., Maccacaro, T., Schild, R. E., & Wolter, A. 1990, ApJ, 348, 141
Strateva, I. V., Brandt, W. N., Schneider, D. P., Vanden Berk, D. G., & Vignali, C. 2005, AJ, 130, 387
Urry, C. M., & Padovani, P. 1995, PASP, 107, 803
Vanden Berk, D. E., et al. 2001, AJ, 122, 549
Vignali, C., Brandt, W. N., Fan, X., Gunn, J. E., Kaspi, S., Schneider, D. P., & Strauss, M. A. 2001, AJ, 122, 2143
Vignali, C., Bauer, F. E., Alexander, D. M., Brandt, W. N., Hornschemeier, A. E., Schneider, D. P., & Garmire, G. P. 2002, ApJ, 580, L105
Vignali, C., Brandt, W. N., Schneider, D. P., Garmire, G. P., & Kaspi, S. 2003a, AJ, 125, 418
Vignali, C., et al. 2003b, AJ, 125, 2876
Vignali, C., Brandt, W. N., Schneider, D. P., & Kaspi, S. 2005, AJ, 129, 2519
Visvanathan, N., & Wills, B. J. 1998, AJ, 116, 2119
Wambsganss, J., Schneider, P., & Paczynski, B. 1990, ApJ, 358, L33
Weinstein, M. A., et al. 2004, ApJS, 155, 243
Wyithe, J. S. B., & Loeb, A. 2002, Nature, 417, 923
York, D. G., et al. 2000, AJ, 120, 1579

TABLE 3
OPTICAL, X-RAY, AND RADIO PROPERTIES

Object (SDSS J) (1)	$N_{\rm H}$[a] (2)	AB_{1450} (3)	M_B (4)	$f_{2500\,\text{Å}}$[b] (5)	$\log(\nu L_\nu)$ 2500 Å (6)	Count Rate[c] (7)	$f_{\rm x}$[d] (8)	$f_{2\,\rm keV}$[e] (9)	$\log(\nu L_\nu)$ 2 keV (10)	$\log L$ 2–10 keV (11)	$\alpha_{\rm ox}$ (12)	$\Delta\alpha_{\rm ox}$ (σ)[f] (13)	R[g] (14)
000239.39+255034.8	4.09	19.0[h]	−28.0	11.8	46.9	$0.85^{+0.58}_{-0.37}$	$3.8^{+2.5}_{-1.7}$	3.86	45.0	45.2	$-1.72^{+0.09}_{-0.10}$	−0.00 (0.0)	< 26.8[o]
000552.34−000655.8	3.14	20.2[h]	−26.8	3.9	46.4	$0.97^{+0.30}_{-0.24}$	$4.2^{+1.3}_{-1.1}$	4.29	45.1	45.3	$-1.52^{+0.06}_{-0.05}$	+0.14 (0.9)	< 51.4
001115.23+144601.8	4.28	18.0[i]	−28.7	29.9	47.2	$28.12^{+3.14}_{-2.83}$	$97.1^{+10.8}_{-9.8}$	86.49	46.3	46.5	$-1.36^{+0.04}_{-0.03}$	+0.40 (3.1)	135.9[o]
084035.09+562419.9	4.37	20.0[j]	−27.0	4.6	46.5	$0.19^{+0.19}_{-0.10}$	$0.8^{+0.8}_{-0.4}$	0.86	44.4	44.6	$-1.81^{+0.12}_{-0.12}$	−0.15 (1.0)	< 11.8
102622.89+471907.0	1.25	18.8[i]	−28.0	14.9	46.9	$1.85^{+1.55}_{-0.91}$[m]	$8.9^{+7.5}_{-4.4}$	7.86	45.2	45.4	$-1.64^{+0.11}_{-0.12}$	+0.08 (0.5)	< 3.0
104845.05+463718.3	1.26	19.3[k]	−27.9	9.5	46.8	$0.20^{+0.20}_{-0.11}$	$0.8^{+0.8}_{-0.4}$	0.86	44.4	44.6	$-1.94^{+0.12}_{-0.12}$	−0.22 (1.4)	< 6.0
105322.98+580412.1	0.56	19.6[i]	−27.3	7.2	46.6	$0.92^{+0.78}_{-0.46}$[m]	$4.3^{+3.7}_{-2.2}$	4.02	45.0	45.2	$-1.63^{+0.11}_{-0.12}$	+0.05 (0.3)	< 7.3
130216.13+003032.1	1.57	19.8[i]	−26.8	5.8	46.4	< 0.44	< 1.4	< 1.14	< 44.3	< 44.5	< −1.81	< −0.16 (> 1.0)	< 8.3
140850.91+020522.7	2.57	18.8[i]	−27.6	14.4	46.7	$4.36^{+1.03}_{-0.85}$	$18.5^{+4.4}_{-3.6}$	13.84	45.3	45.5	$-1.54^{+0.05}_{-0.04}$	+0.16 (1.0)	8.1
141111.29+121737.4	1.69	20.0[h]	−27.1	4.9	46.5	$0.77^{+0.31}_{-0.23}$	$3.2^{+1.3}_{-1.0}$	3.31	45.0	45.2	$-1.60^{+0.07}_{-0.07}$	+0.07 (0.5)	< 13.5
143352.20+022713.9	2.74	18.4[i]	−28.3	20.5	47.0	< 1.37	< 4.5	< 3.84	< 44.9	< 45.1	< −1.81	< −0.08 (> 0.5)	< 2.4
144231.72+011055.2	3.33	20.0[i]	−26.6	4.7	46.3	$3.33^{+0.65}_{-0.55}$	$11.2^{+2.1}_{-1.9}$	9.21	45.2	45.4	$-1.42^{+0.04}_{-0.04}$	+0.22 (1.4)	31.7
153259.96−003944.1	6.60	19.6[l]	−27.0	6.9	46.5	< 0.20[n]	< 0.9	< 0.79	< 44.2	< 44.4	< −1.90	< −0.23 (> 1.5)	< 1.0[p]
153650.26+500810.3	1.57	18.8[i]	−28.0	14.8	46.9	$1.51^{+0.82}_{-0.56}$	$6.2^{+3.4}_{-2.3}$	5.51	45.1	45.3	$-1.70^{+0.08}_{-0.08}$	+0.02 (0.1)	< 3.2
160253.98+422824.9	1.33	19.9[h]	−27.2	5.4	46.6	$1.71^{+0.44}_{-0.36}$	$7.0^{+1.8}_{-1.5}$	7.39	45.3	45.5	$-1.48^{+0.05}_{-0.05}$	+0.20 (1.3)	< 10.3
162331.81+311200.5	2.05	20.1[h]	−27.0	4.2	46.5	$0.17^{+0.17}_{-0.09}$	$0.7^{+0.7}_{-0.4}$	0.75	44.3	44.5	$-1.82^{+0.12}_{-0.14}$	−0.16 (1.0)	< 12.3
162626.50+275132.4	3.27	18.5[i]	−28.4	19.3	47.0	< 1.00	< 4.3	< 4.03	< 45.0	< 45.2	< −1.80	< −0.05 (> 0.4)	< 2.6
163033.90+401209.6	0.86	20.6[k]	−26.4	2.6	46.3	$0.50^{+0.17}_{-0.13}$	$2.0^{+0.7}_{-0.5}$	2.11	44.8	45.0	$-1.57^{+0.06}_{-0.05}$	+0.06 (0.4)	< 19.6
165354.61+405402.1	1.94	19.3[i]	−27.5	9.4	46.7	< 0.96	< 3.1	< 2.77	< 44.8	< 45.0	< −1.74	< −0.05 (> 0.3)	< 5.3
222509.19−001406.8	5.03	19.2[i]	−27.5	10.0	46.7	$0.58^{+0.77}_{-0.37}$	$2.1^{+2.7}_{-1.4}$	1.84	44.6	44.8	$-1.82^{+0.14}_{-0.18}$	−0.12 (0.8)	< 4.7
222845.14−075755.3	4.67	19.1[i]	−27.7	10.9	46.8	$0.28^{+0.38}_{-0.18}$	$1.0^{+1.3}_{-0.7}$	0.92	44.3	44.5	$-1.95^{+0.14}_{-0.20}$	−0.24 (1.6)	< 4.4

[a] Neutral Galactic absorption column density in units of 10^{20} cm^{-2} taken from Dickey & Lockman (1990).
[b] Flux density at rest-frame 2500 Å in units of 10^{-28} erg cm^{-2} s^{-1} Hz^{-1}.
[c] Observed count rate computed in the 0.5–2 keV band in units of 10^{-3} counts s^{-1}.
[d] Galactic absorption-corrected flux in the observed 0.5–2 keV band in units of 10^{-15} erg cm^{-2} s^{-1}.
[e] Flux density at rest-frame 2 keV in units of 10^{-32} erg cm^{-2} s^{-1} Hz^{-1}.
[f] The difference between measured and predicted $\alpha_{\rm ox}$ ($\Delta\alpha_{\rm ox}$), and the significance of that difference (σ), based on the Steffen et al. (2006) $\alpha_{\rm ox}$–$L_\nu(2500\,\text{Å})$ relation.
[g] Unless otherwise noted, radio-to-optical flux ratios (R) involve radio flux densities at an observed-frame frequency of 1.4 GHz taken from the FIRST survey (Becker et al. 1995); upper limits on R are calculated from the 3σ FIRST detection threshold at source position.
[h] Taken from Fan et al. (2004).
[i] Obtained from the SDSS spectrum, corrected for Galactic extinction (Schlegel et al. 1998) and fiber light loss (see § 3).
[j] Taken from Fan et al. (2006).
[k] Taken from Fan et al. (2003).
[l] Estimated as $[(z+0.1)+(i-0.2)]/2$ using the i and z magnitudes in Fan et al. (1999).
[m] Count rate corrected for the exposure map due to a large offset from the aimpoint (see § 2).
[n] Constraints on the count rate and subsequent X-ray parameters were obtained by including an additional *Chandra* exposure (see § 2).
[o] Flux density at an observed-frame frequency of 1.4 GHz taken from the NVSS survey (Condon et al. 1998); upper limits are calculated from the NVSS detection threshold of 2.5 mJy.
[p] Taken from Fan et al. (1999).